Adaptive Linear Turbo Equalization Over Doubly Selective Channels

Jun Won Choi, Thomas J. Riedl, Kyeongyeon Kim, *Member, IEEE*, Andrew C. Singer, *Fellow, IEEE*, and James C. Preisig, *Member, IEEE*

***Abstract*—Over the last decade, tremendous gains, leading to near-capacity achieving performance, have been shown for a variety of communication systems through the application of the *turbo principle*, i.e., the exchange of extrinsic information between constituent algorithms for tasks such as channel decoding, equalization, and multiple-input–multiple-output (MIMO) detection. In this paper, we study the practical application of such an iterative detection and decoding (IDD) framework to underwater acoustic communications. We explore complexity and performance tradeoffs of a variety of turbo equalization (TEQ)-based receiver architectures. First, we elaborate on two popular but suboptimal turbo equalization techniques: a channel-estimate-based minimum mean-square error TEQ (CE-based MMSE-TEQ) and a direct-adaptive TEQ (DA-TEQ). We study the behavior of both TEQ approaches in the presence of channel estimation errors and adaptive filter adjustment errors. We confirm that after a sufficient number of iterations, the performance gap between these two TEQ algorithms becomes small. Next, we demonstrate that an underwater receiver architecture built upon the least mean squares (LMS) DA-TEQ technique can leverage and dramatically improve the performance of the conventional implementation based on the decision-feedback equalizer at a feasible complexity. To maintain performance gains over time-varying channels, the slow convergence speed of the LMS algorithm has been improved via two methods: 1) repeating the weight update for the same set of data with decreasing step size and 2) reducing the dimensionality of the equalizer by capturing sparse channel structure. This receiver architecture was used to process collected data from the *SPACE 08* experiment (Martha's Vineyard, MA). Receiver performance for different modulation orders, channel codes, and hydrophone configurations is examined at a variety of distance, up to 1 km from the transmitters. Experimental results show great promise for this approach, as data rates in excess of 15 kb/s could readily be achieved without error.**

***Index Terms*—Adaptive equalizer, doubly selective channel, iterative receiver, turbo equalization, underwater communication.**

Manuscript received May 12, 2010; revised January 21, 2011; accepted May 19, 2011. Date of publication August 12, 2011; date of current version October 21, 2011.

Associate Editor: M. Stojanovic.

J. W. Choi was with the Coordinated Science Laboratory (CSL), University of Illinois at Urbana-Champaign, Urbana, IL 61801 USA. He is now with Qualcomm QCT, San Diego, CA 92121 USA (e-mail: junwonc@qualcomm.com).

T. J. Riedl and A. C. Singer are with the Coordinated Science Laboratory (CSL), University of Illinois at Urbana-Champaign, Urbana, IL 61801 USA (e-mail: tomj.riedl@gmail.com; acsinger@illinois.edu).

K. Kim was with the Coordinated Science Laboratory (CSL), University of Illinois at Urbana-Champaign, Urbana, IL 61801 USA. She is now with Samsung Advanced Institute of Technology (SAIT), Yongin-si Gyeonggi-do 445-160, Korea (e-mail: adrianakky@gmail.com;).

J. C. Preisig is with the Department of Applied Ocean Physics and Engineering, Woods Hole Oceanographic Institution, Woods Hole, MA 02543-1050 USA (e-mail: jpreisig@whoi.edu).

Color versions of one or more of the figures in this paper are available online at http://ieeexplore.ieee.org.

Digital Object Identifier 10.1109/JOE.2011.2158013

I. Introduction

To achieve reliable communication over wireless channels, intersymbol interference (ISI) caused by delay spread of the channel should be mitigated by an equalization technique. For decades, equalization techniques for a variety of ISI channels have been established in the literature [1]. However, the performance of equalization methods is often limited when the channel is rapidly time varying or poorly modeled. An example of such a challenging channel is the *underwater acoustic channel*. Fig. 1 shows a time-delay response of an underwater channel for 1-km distance from the transmitter. It is observed that at a symbol rate of 9.77 ksymbol/s, the channel response spans around 70 symbols. When a hydrophone array with multiple elements is deployed, the number of unknown parameters for the equalization task can run into the thousands, which demands tremendous complexity for equalization. In addition, the increase in the number of unknown parameters makes the tracking of fast channel variations difficult. One approach to lower the equalization complexity is to use an orthogonal frequency division multiplexing (OFDM) transmission, which transforms a tapped-delay-line channel response to parallel scalar channel gains [2]. By performing separate scalar equalization for each subcarrier, the complexity of the receiver can be significantly reduced. Unfortunately, for rapidly varying channels such as an underwater acoustic channel, these approaches often suffer from an intercarrier interference (ICI), which degrades the system performance [3].

To approach the performance of the joint equalization and decoding, the turbo equalization (TEQ) technique motivated by the turbo principle [4] was introduced. The TEQ technique exploits information obtained from a channel decoder to improve equalization [5]–[11]. Exchange of soft information between the equalizer and the channel decoder is carried out in an iterative fashion until the performance ceases to improve. In [5], a TEQ algorithm is derived by computing *a posteriori* log-likelihood ratio (LLR) of the data bits directly using received data and *a priori* LLRs obtained from the channel decoder. Since direct computation of *a posteriori* LLRs requires prohibitive complexity, various low-complexity TEQ techniques have been proposed. In [6], a linear adaptive TEQ is introduced, where soft symbol estimates are fed back to the equalizer and the equalizer coefficients are adjusted to minimize mean square error (MSE) in an adaptive fashion. A linear minimum mean square error (MMSE) TEQ was investigated in [7] and [8], where a linear MMSE equalizer was derived given exact knowledge of the channel. Without knowledge of the channel state,

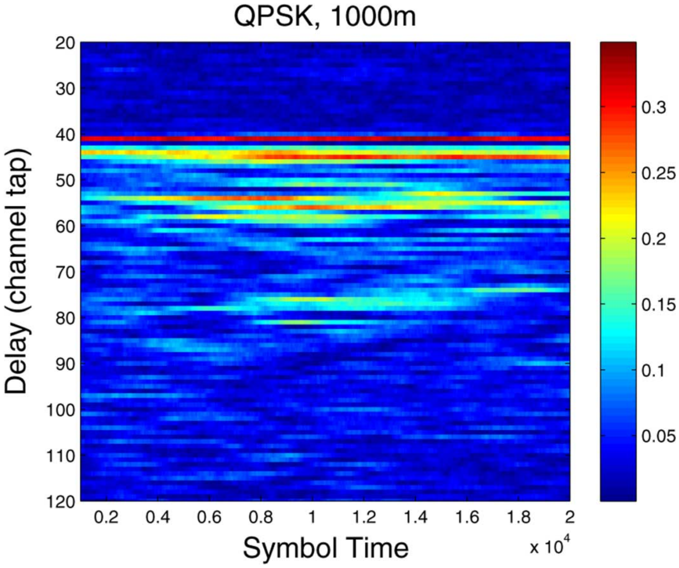

Fig. 1. The plot of channel estimates. A colormap is used to represent magnitude of channel gains over time-delay domain.

the channel could be estimated and the estimates incorporated into the equalizer. Since channel estimation errors deteriorate equalization performance, the covariance matrix of the channel estimation errors can be accounted for in the derivation of the linear MMSE equalizer to reduce the impact of channel estimation errors as in [9]. In [10] and [11], a low-complexity implementation of joint channel estimation and equalization approaches are investigated. The application of similar iterative detection schemes can be found in other digital communication problems such as multiuser detection [12], multiple-input–multiple-output (MIMO) detection [13]–[15], and ICI cancellation for OFDM system [3].

Recently, TEQ techniques have been applied to underwater acoustic communications [16]–[22]. Iterative detection algorithms were derived for multichannel equalization in [16] and [17] and extensive experimental results for the turbo receiver were presented in [18]. A low-complexity turbo equalizer was presented for systems employing space-time codes in [19] and a nonlinear TEQ technique followed by a prefiltering (channel-shaping) filter was proposed in [20]. In [21], multicarrier transmission is considered to reduce the effective channel length for low-complexity implementation of TEQ. In [22], a Markov chain Monte Carlo (MCMC) turbo equalizer is also developed to bridge the gap between the complex nonlinear maximum *a posteriori* (MAP) equalizer and linear TEQ algorithm.

In this paper, we study the practical application of linear TEQ techniques to underwater acoustic communications. We conduct comparative study on two well-known linear turbo equalizers and present experimental results with field data. First, we investigate two popular TEQ algorithms with linear structure: 1) a channel-estimate-based MMSE TEQ (CE-based MMSE-TEQ) technique and 2) a direct-adaptive TEQ (DA-TEQ) technique. The CE-based MMSE-TEQ algorithm exploits an explicit channel estimate to determine the equalizer coefficients. In contrast, the DA-TEQ algorithm directly estimates a symbol using well-known adaptive algorithms [23]. Since both TEQ algorithms are suboptimal without knowledge of the channel, it is of interest to take a close look at their differences. Basically, two TEQ algorithms operate on different criteria; while the CE-based MMSE-TEQ algorithm minimizes the conditional MSE for given *a priori* information on symbols and the estimated channel, DA-TEQ minimizes the unconditional MSE due to the autonomous nature of adaptive algorithms. As a result, the coefficients of the DA-TEQ do not capture time-varying second-order symbol statistics, and hence its optimal Wiener solution to which they approach is different from that of the optimal MMSE-TEQ. We compare the behavior of the CE-based MMSE-TEQ and DA-TEQ algorithms in the presence of channel estimation errors and adjustment errors of the least mean squares (LMS) adaptive algorithm used in the implementation. In spite of the discrepancy of their respective optimal forms, we show through extrinsic information transfer (EXIT) chart analysis that the performance gap between the DA-TEQ and CE-based MMSE-TEQ techniques is small after convergence.

Next, we introduce an underwater acoustic communication receiver architecture based on the DA-TEQ technique. An LMS adaptive algorithm is used to maintain low equalization complexity. To facilitate good tracking performance for the LMS DA-TEQ algorithm, we improve the convergence speed of the LMS algorithm by two methods: 1) repeating the weight update over blocks of the same set of data ("data reuse LMS" [24]) with decreasing step size ("gear shifting LMS" [25], [26]) and 2) reducing the number of active equalizer taps based on the sparse structure of the underwater acoustic channel. With the aid of these means, the LMS DA-TEQ technique can show better decoding results than the original form of the LMS turbo equalizer [6] in real underwater channels. The performance of our receiver architecture was tested via the *SPACE 08* experiment conducted off the coast of Martha's Vineyard, MA. We show that a substantial performance gain can be achieved over the conventional decision feedback equalizer widely adopted for underwater acoustic communication modems [27].

It is worth mentioning that we have attempted a challenging transmission setup, i.e., signal transmission beyond the Nyquist signaling rate. To increase the data rate under a bandwidth constraint, we pushed the symbol rate beyond that which would yield no ISI at the transmitter, that is, twice the transmission bandwidth $2W$ [28]. This generates *artificial* ISI, consequently increasing the effective channel span at the receiver and degrading the receiver performance. We will show that the LMS DA-TEQ technique maintains strong performance even in this challenging environment, offering the best data rate among all configurations considered.

The rest of this paper is organized as follows. In Section II, the overall system is described. In Section III, TEQ techniques with linear structure are briefly described, and in Section IV, the performance of two practical linear TEQ algorithms are compared: CE-based MMSE-TEQ technique and DA-TEQ technique. In Section V, an underwater receiver architecture based on the LMS DA-TEQ algorithm is introduced. In Section VI, the experimental results are discussed, and in Section VII, some conclusions are discussed.

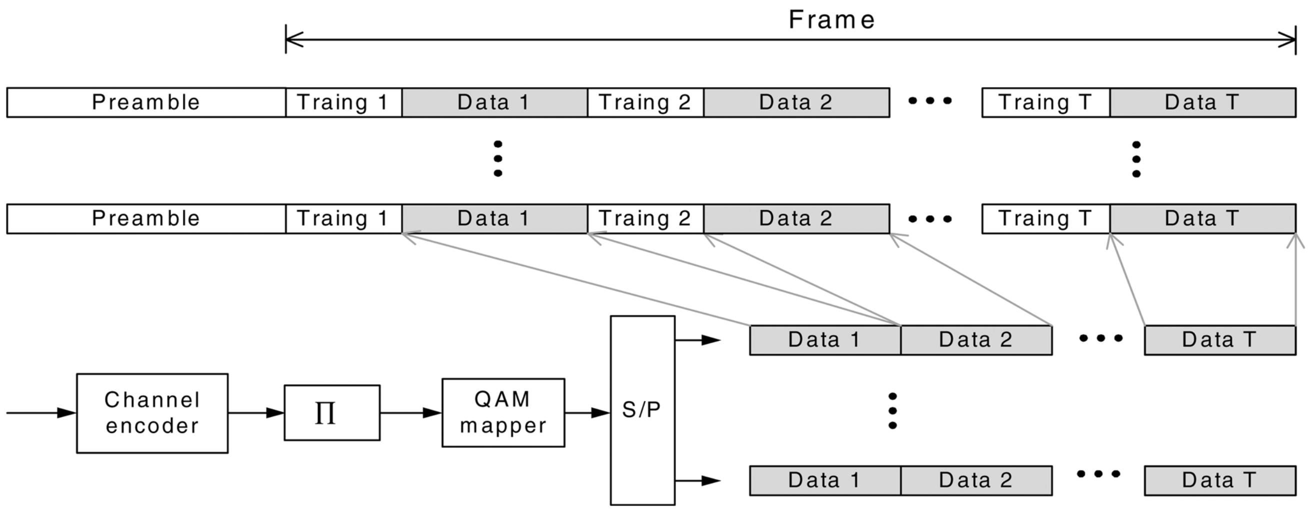

Fig. 2. Frame structure.

II. System Description

A. Notation

The notation to be used in the rest of paper is summarized as follows.

- Uppercase and lowercase letters written in boldface are used for matrix and vector notation, respectively.
- $\mathcal{CN}(\mathbf{m}, \mathbf{\Sigma})$ is a complex Gaussian distribution with the mean $\mathbf{m}$ and the covariance matrix $\mathbf{\Sigma}$, and $\mathcal{N}(\mathbf{m}, \mathbf{\Sigma})$ is a real Gaussian distribution.
- $\mathbf{1}_{i\times j}$ is the $i \times j$ matrix where entries are all one. $\mathbf{0}_{i\times j}$ is a zero matrix defined similarly. Note that $\mathbf{1}_i$ and $\mathbf{0}_i$ represent an $i \times i$ square matrix. The subscript for these matrices can be omitted without risk of confusion.
- $\mathrm{diag}\{x_1, \ldots, x_n\}$ is a diagonal matrix whose diagonals are $x_1, \ldots, x_n$.
- $\mathrm{Var}(x) = E[x^2] - E[x]^2$. $\mathrm{Cov}(\mathbf{x}) = E[(\mathbf{x} - E[\mathbf{x}])(\mathbf{x} - E[\mathbf{x}])^H]$ and $\mathrm{Cov}(\mathbf{x}, \mathbf{y}) = E[(\mathbf{x} - E[\mathbf{x}])(\mathbf{y} - E[\mathbf{y}])^H]$.
- $\mathrm{tr}(\cdot)$ denotes a trace operation.

B. Transmitter Description

The transmitter structure considered here is based on space-time bit-interleaved coded modulation (ST-BICM) [29], which allows us to perform coding over different temporal and spatial dimensions. First, the information bits $\{b_k\}$ are encoded by a rate R_c channel encoder, producing the coded bit sequence $\{c_i\}$. The sequence $\{c_i\}$ is permuted using a random interleaver and Q interleaved bits are mapped to 2^Q-ary quadrature amplitude modulation (QAM) symbols. The sequence of the QAM symbols is divided into N_t parallel streams using a serial-to-parallel converter. These parallel data streams are transmitted through a transmitter array with N_t elements. In the following, we denote $x_{m,n}$ as a symbol sent by the mth array element at time n. We also denote the Q coded bits that are mapped to $x_{m,n}$ via QAM as $\bar{c}^1_{m,n}, \ldots, \bar{c}^Q_{m,n}$. For convenience, we assume that a coded bit $\bar{c}^q_{m,n}$ has ± 1 value instead of a binary number.

Data transmission is carried out frame by frame. As shown in Fig. 2, a frame consists of T sets of the training symbols followed by the data symbols. The preamble symbols are inserted in front of every multiple frame for data acquisition and synchronization purposes. The training symbols are used to aid tracking performance of the adaptive equalizer or channel estimator. The periods of training, data, and preamble sequences are M_t, M_d, and M_p symbol times, respectively.

C. Receiver Description

Assuming perfect synchronization and symbol-spaced sampling, the signal received at the hydrophone array with N_r elements is expressed as

$$\mathbf{r}_n = \sum_{k=-K_f}^{K_p} \mathbf{H}_{n,k}\mathbf{x}_{n-k} + \mathbf{w}_n \tag{1}$$

where n and k are time and delay indices, respectively. Note that $\mathbf{r}_n$ and $\mathbf{w}_n$ are the $N_r \times 1$ received and noise vectors, respectively, $\mathbf{x}_n = [x_{1,n}, \ldots, x_{N_t,n}]^T$, and $\mathbf{H}_{n,k}$ is the $N_r \times N_t$ matrix whose (l, m)th element is the channel gain from the mth transmitter element to the lth receiver element. The channel length is assumed to be at most $K_f + K_p + 1$, where K_f is the length of the precursor and K_p is that of the postcursor response. We also assume that channel gains change in time n. The signal vector $\mathbf{x}_n$ is normalized to have unit energy and assumed to be uncorrelated due to the interleaver, i.e., $E[\mathbf{x}_n\mathbf{x}_n^H] = \mathbf{I}_{N_t}$. Considering an observation window containing $L_f + L_p + 1$ received vectors, i.e., $\mathbf{r}_{n-L_p}, \ldots, \mathbf{r}_{n+L_f}$, we can write

$$\mathbf{y}_n = \mathbf{H}_n\mathbf{s}_n + \mathbf{n}_n \tag{2}$$

where

$$\mathbf{y}_n = \left[\mathbf{r}^T_{n+L_f}, \ldots, \mathbf{r}^T_{n-L_p}\right]^T, \quad \mathbf{n}_n = \left[\mathbf{w}^T_{n+L_f}, \ldots, \mathbf{w}^T_{n-L_p}\right]^T$$

$$\mathbf{s}_n = \left[\mathbf{x}^T_{n+K_f+L_f}, \ldots, \mathbf{x}^T_{n-K_p-L_p}\right]^T$$

$$\mathbf{H}_n = \begin{bmatrix} \mathbf{H}_{n+L_f,-K_f} & \cdots & \mathbf{H}_{n+L_p,K_p} & \mathbf{0} & \mathbf{0} \\ \mathbf{0} & \ddots & \cdots & \ddots & \mathbf{0} \\ \mathbf{0} & \mathbf{0} & \mathbf{H}_{n-L_p,-K_f} & \cdots & \mathbf{H}_{n-L_p,K_p} \end{bmatrix}.$$

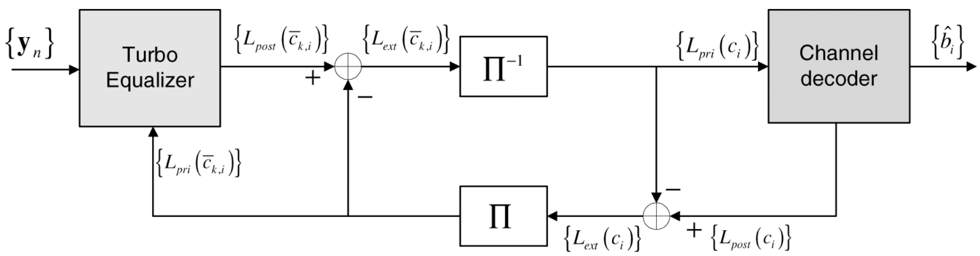

Fig. 3. Block diagram of the receiver architecture. $\prod$ and $\prod^{-1}$ denote interleaving and deinterleaving operations, respectively.

The vector $\mathbf{y}_n$ contains all received vectors in the observation window and the noise vector $\mathbf{n}_n$ is assumed to be complex Gaussian, i.e., $\mathbf{n}_n \sim \mathcal{CN}(\mathbf{0}, \mathbf{R})$. In the following, we will denote

$$K = N_t(K_p + K_f + L_p + L_f + 1)$$

and

$$L = N_r(L_p + L_f + 1)$$

so that the size of $\mathbf{H}_n$ becomes $L \times K$. For convenience, we also denote

$$\mathbf{s}_n = [s_{n,1}, \ldots, s_{n,K}]^T$$
$$\mathbf{y}_n = [y_{n,1}, \ldots, y_{n,L}]^T$$

and

$$\mathbf{H}_n = [\mathbf{h}_{n,1}, \ldots, \mathbf{h}_{n,K}].$$

In addition, we let $\mathbf{H}_{n,i:j} = [\mathbf{h}_{n,i}, \mathbf{h}_{n,i+1} \ldots, \mathbf{h}_{n,j}]$ for $i < j$.

A block diagram of the TEQ system is shown in Fig. 3. The equalizer produces extrinsic LLRs on the coded bits using the received vector $\mathbf{y}_n$ and the *a priori* LLRs on them [7], [8]. Specifically, the extrinsic LLR $L_{\rm ext}(\bar{c}^q_{n,k})$ can be obtained from

$$L_{\rm ext}(\bar{c}^q_{n,k}) = L_{\rm post}(\bar{c}^q_{n,k}) - L_{\rm pri}(\bar{c}^q_{n,k})$$

where $L_{\rm pri}(\bar{c}^q_{n,k})$ is the *a priori* LLR defined as

$$L_{\rm pri}(\bar{c}^q_{n,k}) = \ln Pr(\bar{c}^q_{n,k} = +1) - \ln Pr(\bar{c}^q_{n,k} = -1)$$

and $L_{\rm post}(\bar{c}^q_{n,k})$ is the *a posteriori* LLR defined as

$$L_{\rm post}(\bar{c}^q_{n,k}) = \ln Pr(\bar{c}^q_{n,k} = +1|\text{observation}) - \ln Pr(\bar{c}^q_{n,k} = -1|\text{observation}).$$

Note that the observation can be any function of $\mathbf{y}_n$ and the *a priori* LLRs are obtained from the channel decoder. The extrinsic LLRs produced in the equalizer are delivered to the channel decoder through the deinterleaver. They are used as *a priori* LLRs to produce the additional extrinsic LLRs in the channel decoder. Finally, the extrinsic LLRs obtained by the channel decoder are fed back to the equalizer after being converted to the *a priori* LLRs by the interleaver. These steps complete one cycle of turbo iteration and are repeated until a suitably chosen convergence criterion is achieved.

III. Review of Turbo Equalizer With Linear Structure

In what follows, we briefly review three different linear TEQ techniques: 1) MMSE-TEQ, 2) CE-based MMSE-TEQ, and 3) DA-TEQ. The MMSE-TEQ technique minimizes an MSE criterion under the condition that the channel state is perfectly known. When the channel is not known, two alternative TEQ techniques are available: the CE-based MMSE-TEQ and the DA-TEQ. Though these two algorithms are suboptimal, they are adopted for practical systems due to relatively low computational complexity.

A. MMSE Turbo Equalizer

With perfect knowledge of the channel matrix $\mathbf{H}_n$, a linear MMSE estimate of the symbol $s_{n,k}$ for $k \in [N_t(K_f + L_f) + 1, N_t(K_f + L_f) + N_t]$ is given by [7]

$$\begin{aligned}\hat{s}^{\rm MMSE}_{n,k} &= \mathbf{z}^H_{n,k}(\mathbf{y}_n - \mathbf{H}_n\bar{\mathbf{s}}_{n,k})\\ \mathbf{z}_{n,k} &= (\mathbf{H}_n\mathbf{\Sigma}_{n,k}\mathbf{H}^H_n + \mathbf{R})^{-1}\mathbf{h}_{n,k}\end{aligned} \tag{3}$$

where

$$\bar{\mathbf{s}}_{n,k} = [\bar{s}_{n,1}, \ldots, \bar{s}_{n,k-1}, 0, \bar{s}_{n,k+1}, \ldots \bar{s}_{n,K}]^T$$
$$\mathbf{\Sigma}_{n,k} = \text{diag}(\lambda_{n,1}, \ldots, \lambda_{n,k-1}, 1, \lambda_{n,k+1}, \ldots, \lambda_{n,K})$$

are a mean vector and covariance matrix of $\mathbf{s}_n$ for given *a priori* LLRs.

To prevent the decoder from using the information that it already knows, the linear MMSE estimate in (3) does not rely on *a priori* knowledge of $s_{n,k}$, i.e., $\bar{s}_{n,k} = 0$ and $\lambda_{n,k} = 1$. We can obtain $\bar{s}_{n,i}$ and $\lambda_{n,i}$ from *a priori* LLRs as [7]

$$\bar{s}_{n,i} = \sum_{\theta\in\Theta} \theta \prod_{q=1}^{Q} \frac{1}{2}\left(1 + \bar{c}^q_{n,i}\tanh\left(\frac{L_{\rm pri}(\bar{c}^q_{n,i})}{2}\right)\right) \tag{4}$$

$$\lambda_{n,i} = \sum_{\theta\in\Theta} |\theta|^2 \prod_{q=1}^{Q} \frac{1}{2}\left(1 + \bar{c}^q_{n,i}\tanh\left(\frac{L_{\rm pri}(\bar{c}^q_{n,i})}{2}\right)\right) - |\bar{s}_{n,i}|^2 \tag{5}$$

where Θ is the set of all constellation points for 2^Q-ary QAM. A simpler expression of $\bar{\mathbf{s}}_{n,k}$ and $\mathbf{\Sigma}_{n,k}$ is available for a particular signal mapper [8]. By treating the MMSE estimate $\hat{s}^{\rm MMSE}_{n,k}$ as an observation, we can compute the extrinsic LLR for $\bar{c}^q_{n,k}$ as follows. From (2) and (3), we can express $\hat{s}^{\rm MMSE}_{n,k}$ as a sum of a signal part and a residual error part, i.e., $\hat{s}_{n,k}^{\mathrm{MMSE}} = \mu_{n,k}s_{n,k} + \eta_{n,k}$, where

$$\mu_{n,k} = \mathbf{z}_{n,k}^H \mathbf{h}_{n,k} \quad (6)$$

$$\eta_{n,k} = \mathbf{z}_{n,k}^H (\mathbf{H}_n(\mathbf{s}_n - \bar{\mathbf{s}}_{n,k}) - \mathbf{h}_{n,k}s_{n,k} + \mathbf{n}_n). \quad (7)$$

We can show $\mathrm{Var}(\eta_{n,k}) \triangleq \sigma_{n,k}^2 = \mu_{n,k}(1-\mu_{n,k})$ [7]. If we make the widely used assumption that $\eta_{n,k}$ is Gaussian, i.e., $\eta_{n,k} \sim \mathcal{CN}(0, \sigma_{n,k}^2)$, the extrinsic LLR of $\bar{c}_{n,k}^q$ is given by (8) and (9), shown at the bottom of the page, where $\Theta_{k,q}^{+1}$ and $\Theta_{k,q}^{-1}$ are the set of all constellation points such that $\bar{c}_{n,k}^q$ is $+1$ and -1, respectively.

B. CE-Based MMSE-TEQ

When perfect channel knowledge is not available, the channel response can be estimated and incorporated into the coefficients of the MMSE-TEQ algorithm. Define the channel estimate $\hat{\mathbf{H}}_n$ and the corresponding channel estimation error $\mathbf{E}_n = \mathbf{H}_n - \hat{\mathbf{H}}_n$. We assume that $\mathbf{E}_n$ has zero mean and is uncorrelated with $\hat{\mathbf{H}}_n$. We assume that $\mathbf{E}_n$ is also uncorrelated with $\mathbf{s}_n$. Then, we can write (2) by $\mathbf{y}_n = \hat{\mathbf{H}}_n\mathbf{s}_n + (\mathbf{E}_n\mathbf{s}_n + \mathbf{n}_n)$. Given the channel estimate $\hat{\mathbf{H}}_n$, the linear MMSE estimate of $s_{n,k}$ is given by

$$\hat{s}_{n,k}^{\mathrm{CE-MMSE}} = \hat{\mathbf{z}}_{n,k}^H \left(\mathbf{y}_n - \hat{\mathbf{H}}_n\bar{\mathbf{s}}_{n,k}\right)$$

$$\hat{\mathbf{z}}_{n,k} = \left(\hat{\mathbf{H}}_n\mathbf{\Sigma}_{n,k}\hat{\mathbf{H}}_n^H + E\left[\mathbf{E}_n\mathbf{E}_n^H\right] + \mathbf{R}\right)^{-1}\hat{\mathbf{h}}_{n,k}. \quad (10)$$

Note that the term $E[\mathbf{E}_n\mathbf{E}_n^H]$ can be obtained from an analysis of the channel estimator. Alternatively, we can estimate the sum $E[\mathbf{E}_n\mathbf{E}_n^H] + \mathbf{R}$ by

$$E\left[\mathbf{E}_n\mathbf{E}_n^H\right] + \mathbf{R} \approx \frac{1}{M_t}\sum_{n=1}^{M_t}(\mathbf{y}_n - \hat{\mathbf{H}}_n\mathbf{s}_n)(\mathbf{y}_n - \hat{\mathbf{H}}_n\mathbf{s}_n)^H \quad (11)$$

where $\mathbf{s}_n$ is obtained from training data. Denoting

$$\hat{\mu}_{n,k} = \hat{\mathbf{z}}_{n,k}^H\hat{\mathbf{h}}_{n,k}$$

we can express

$$\hat{s}_{n,k}^{\mathrm{CE-MMSE}} = \hat{\mu}_{n,k}s_{n,k} + \hat{\eta}_{n,k}$$

where $\mathrm{Var}(\hat{\eta}_{n,k}) = \hat{\mu}_{n,k}(1-\hat{\mu}_{n,k})$. Hence, the extrinsic LLR for $\bar{c}_{n,k}^q$ is given by (12), shown at the bottom of the page.

C. Direct-Adaptive Turbo Equalizer (DA-TEQ)

We can estimate the symbol s_k directly via an adaptive algorithm. First, we restrict the estimate of s_k to be a linear combination of observations and *a priori* symbol estimates, i.e., [6]

$$\hat{s}_{n,k}^{\mathrm{DA}} = \mathbf{f}_{n,k}^H\mathbf{y}_n + \mathbf{g}_{n,k}^H\begin{bmatrix}\bar{\mathbf{s}}_{n,1:k-1}\\ \bar{\mathbf{s}}_{n,k+1:K}\end{bmatrix} \quad (13)$$

where $\bar{\mathbf{s}}_{n,i:j} = [\bar{s}_{n,i}, \ldots, \bar{s}_{n,j}]^T$ for $i < j$. The vectors $\mathbf{f}_{n,k}$ and $\mathbf{g}_{n,k}$ represent the $L \times 1$ feedforward and $(K-1) \times 1$ feedback coefficients, respectively. These coefficients are adjusted such that the MSE $E[|s_{n,k} - \hat{s}_{n,k}^{\mathrm{DA}}|^2]$ is minimized. We can update these coefficients via an LMS algorithm, i.e.,

$$\begin{bmatrix}\mathbf{f}_{n+1,k}\\ \mathbf{g}_{n+1,k}\end{bmatrix} = \begin{bmatrix}\mathbf{f}_{n,k}\\ \mathbf{g}_{n,k}\end{bmatrix} + \xi\left(s_{n,k} - \hat{s}_{n,k}^{\mathrm{DA}}\right)\begin{bmatrix}\mathbf{y}_n\\ \bar{\mathbf{s}}_{n,1:k-1}\\ \bar{\mathbf{s}}_{n,k+1:K}\end{bmatrix} \quad (14)$$

$$L_{\mathrm{ext}}^{\mathrm{MMSE}}\left(\bar{c}_{n,k}^q\right) = \ln\frac{P\left(\bar{c}_{n,k}^q = +1 \,\middle|\, \hat{s}_{n,k}^{\mathrm{MMSE}}\right)}{P\left(\bar{c}_{n,k}^q = -1 \,\middle|\, \hat{s}_{n,k}^{\mathrm{MMSE}}\right)} - \ln\frac{P\left(\bar{c}_{n,k}^q = +1\right)}{P\left(\bar{c}_{n,k}^q = -1\right)} \quad (8)$$

$$= \ln\frac{\sum_{\theta\in\Theta_q^{+1}}\exp\left(-\frac{\left|\hat{s}_{n,k}^{\mathrm{MMSE}} - \mu_{n,k}\theta\right|^2}{\sigma_{n,k}^2} + \frac{1}{2}\sum_{i=1,i\neq q}^{Q}\bar{c}_{n,k}^i L_{\mathrm{pri}}\left(\bar{c}_{n,k}^i\right)\right)}{\sum_{\theta\in\Theta_q^{-1}}\exp\left(-\frac{\left|\hat{s}_{n,k}^{\mathrm{MMSE}} - \mu_{n,k}\theta\right|^2}{\sigma_{n,k}^2} + \frac{1}{2}\sum_{i=1,i\neq q}^{Q}\bar{c}_{n,k}^i L_{\mathrm{pri}}(\bar{c}_{n,k}^i)\right)} \quad (9)$$

$$L_{\mathrm{ext}}^{\mathrm{CE-MMSE}}\left(\bar{c}_{n,k}^q\right) = \ln\frac{\sum_{\theta\in\Theta_q^{+1}}\exp\left(-\frac{\left|\hat{s}_{n,k}^{\mathrm{CE-MMSE}} - \hat{\mu}_{n,k}\theta\right|^2}{\hat{\mu}_{n,k}(1-\hat{\mu}_{n,k})} + \frac{1}{2}\sum_{i=1,i\neq q}^{Q}\bar{c}_{n,k}^i L_{\mathrm{pri}}(\bar{c}_{n,k}^i)\right)}{\sum_{\theta\in\Theta_q^{-1}}\exp\left(-\frac{\left|\hat{s}_{n,k}^{\mathrm{CE-MMSE}} - \hat{\mu}_{n,k}\theta\right|^2}{\hat{\mu}_{n,k}(1-\hat{\mu}_{n,k})} + \frac{1}{2}\sum_{i=1,i\neq q}^{Q}\bar{c}_{n,k}^i L_{\mathrm{pri}}(\bar{c}_{n,k}^i)\right)}. \quad (12)$$

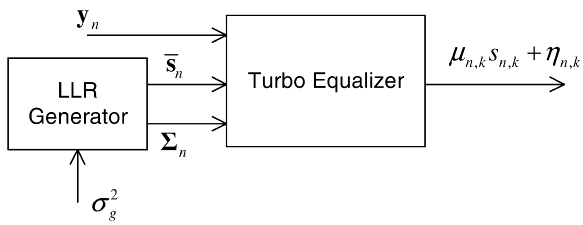

Fig. 4. Setup for performance analysis.

where ξ is a step size. When $s_{n,k}$ is not available, a tentative symbol estimate $Q(\hat{s}_{n,k}^{\mathrm{DA}})$ can be used in place of $s_{n,k}$ in (14), where $Q(\cdot)$ is the slicer operation that maps the input to the nearest constellation point. Note that to obtain $\hat{s}_{n,k}^{\mathrm{DA}}$ for all

$$k \in [N_t(K_f+L_f)+1, N_t(K_f+L_f)+N_t]$$

the DA-TEQ updates N_t feedforward and feedback filters separately.

Computation of the extrinsic LLR from the output of the DA-TEQ is not straightforward since the channel response, and equivalently $\mu_{n,k}$ and $\sigma_{n,k}^2$ in (9) are not known. An approximate soft demapping algorithm for obtaining the extrinsic LLR in the DA-TEQ was proposed in [6]. In Section V, we will present a different soft demapping algorithm for our receiver architecture.

IV. Comparison of CE-Based MMSE-TEQ Versus LMS DA-TEQ

In this section, we compare the performance of the CE-based MMSE-TEQ and the LMS DA-TEQ techniques. To simplify the analysis, we assume a locally time-invariant channel, i.e., $\mathbf{H}_n = \mathbf{H}$ for n. Following the methodology used in [30], we model the *a priori* LLR as a conditional Gaussian variable, i.e.,

$$L_{\mathrm{pri}}(\bar{c}_{n,k}^q) \sim \mathcal{N}(\sigma_g^2/2, \sigma_g^2)$$

for $\bar{c}_{n,k}^q = +1$ and

$$L_{\mathrm{pri}}(\bar{c}_{n,k}^q) \sim \mathcal{N}(-\sigma_g^2/2, \sigma_g^2)$$

for $\bar{c}_{n,k}^q = -1$. Hence, the distribution of the *a priori* LLR is characterized by the single parameter σ_g^2. In the analysis that follows, *a priori* LLR is seen as a random signal that is correlated with $\bar{c}_{n,k}^q$. Since $\bar{\mathbf{s}}_n$ and $\boldsymbol{\Sigma}_n$ are functions of the *a priori* LLR [see (4) and (5)], they are also random signals characterized by σ_g^2. We will consider in the analysis that *a priori* LLRs provide *side information* on $\bar{c}_{n,k}^q$ denoted as $\mathcal{L}$. As the parameter σ_g^2 increases, this side information becomes more reliable. Denoting $\bar{\mathbf{s}}_n = E[\mathbf{s}_n|\mathcal{L}]$, we have $E[\bar{\mathbf{s}}_n] = \mathbf{0}_{K\times 1}$ and $\mathrm{Cov}(\mathbf{s}_n - \bar{\mathbf{s}}_n, \bar{\mathbf{s}}_n^H) = \mathbf{0}_K$ due to the orthogonality principle. In addition, with $\mathrm{Cov}(\bar{\mathbf{s}}_n) \triangleq \sigma_{\bar{s}}^2\mathbf{I}_K$, we have

$$\mathrm{Cov}(\mathbf{s}_n - \bar{\mathbf{s}}_n) = (1-\sigma_{\bar{s}}^2)\mathbf{I}_K.$$

The framework under which the analysis is performed is depicted in Fig. 4.

A. MSE Analysis

First, we look at the performance of the CE-based MMSE-TEQ technique. Given the side information $\mathcal{L}$ and the channel estimate $\hat{\mathbf{H}}_n$, the CE-based MMSE-TEQ algorithm minimizes the conditional MSE, i.e.,

$$E\left[\left|s_{n,k} - \hat{s}_{n,k}^{\mathrm{CE-MMSE}}\right|^2 \middle| \mathcal{L}, \hat{\mathbf{H}}_n\right] = 1 - \hat{\mathbf{h}}_{n,k}^H\left(\hat{\mathbf{H}}_n\boldsymbol{\Sigma}_{n,k}\hat{\mathbf{H}}_n^H + E\left[\mathbf{E}_n\mathbf{E}_n^H\right] + \mathbf{R}\right)^{-1}\hat{\mathbf{h}}_{n,k}. \quad (15)$$

We assume that the channel estimation error $(\hat{\mathbf{H}}_n - \mathbf{H})$ is a random matrix uncorrelated with $\hat{\mathbf{H}}_n$. To obtain an average MSE, (15) should be averaged over $\boldsymbol{\Sigma}_{n,k}$ and $\hat{\mathbf{H}}_n$, i.e.,

$$E\left[|s_{n,k} - \hat{s}_{n,k}^{\mathrm{CE-MMSE}}|^2\right] = 1 - E \times\left[\hat{\mathbf{h}}_{n,k}^H\left(\hat{\mathbf{H}}_n\boldsymbol{\Sigma}_{n,k}\hat{\mathbf{H}}_n^H + E\left[\mathbf{E}_n\mathbf{E}_n^H\right] + \mathbf{R}\right)^{-1}\hat{\mathbf{h}}_{n,k}\right]. \quad (16)$$

Consider a standard LMS channel estimator with a step size ξ_{ch} estimating $K_p + K_f + 1$ channel taps. The covariance matrix of the channel estimation error is given by

$$(\xi_{\mathrm{ch}})/(2)(\mathrm{tr}(\mathbf{R}))/(L)\mathbf{I}_{K_p+K_f+1}$$

(see Appendix I). Assuming that $\hat{\mathbf{H}}_n - \mathbf{H}$ is complex Gaussian, we can obtain (16) by generating random samples of $\hat{\mathbf{H}}_n$ and performing *Monte Carlo* averaging.

Next, we take a look at the performance of the LMS DA-TEQ algorithm. Contrary to the CE-based MMSE-TEQ algorithm, the LMS DA-TEQ algorithm minimizes the unconditional MSE, i.e., $E[|s_{n,k} - \hat{s}_{n,k}^{\mathrm{LMS-DA}}|^2]$ via the LMS algorithm. At first, we look at the Wiener solution to which the coefficients of the LMS DA-TEQ converge in mean square sense. Let the converged feedback and feedforward coefficients be $\mathbf{g}_k^o$ and $\mathbf{f}_k^o$, respectively. Using the orthogonality principle between $s_n - \hat{s}_n^{\mathrm{LMS-DA}}$ and $[\bar{\mathbf{s}}_{n,1:k-1}^T, \bar{\mathbf{s}}_{n,k+1:K}^T]^T$, we have

$$\mathbf{g}_{n,k} \longrightarrow \mathbf{g}_k^o = -\left[\mathbf{H}_{n,1:k-1} \quad \mathbf{H}_{n,k+1:K}\right]^H\mathbf{f}_k^o. \quad (17)$$

In a similar manner, using that $s_{n,k} - \hat{s}_{n,k}^{\mathrm{LMS-DA}}$ and $\mathbf{y}_n$ are uncorrelated, we get

$$\mathbf{f}_{n,k} \longrightarrow \mathbf{f}_k^o = \left(\mathbf{h}_{n,k}\mathbf{h}_{n,k}^H + (1-\sigma_{\bar{s}}^2)\mathbf{H}_{n,1:k-1}\mathbf{H}_{n,1:k-1}^H + (1-\sigma_{\bar{s}}^2)\mathbf{H}_{n,k+1:K}\mathbf{H}_{n,k+1:K}^H + \mathbf{R}\right)^{-1}\mathbf{h}_{n,k}. \quad (18)$$

From (13), (17), and (18), we can show that the output of LMS DA-TEQ converges to

$$\hat{s}_{n,k}^{\mathrm{LMS-DA}} \longrightarrow \left(\mathbf{f}_k^o\right)^H(\mathbf{y}_n - \mathbf{H}_n\bar{\mathbf{s}}_{n,k}). \quad (19)$$

We can compare this Wiener solution with the optimal MMSE solution in (3). Clearly, the optimal MMSE-TEQ and DA-TEQ share the same structure; the soft feedback estimates are subtracted from the observation, i.e., $\mathbf{y}_n - \mathbf{H}_n\bar{\mathbf{s}}_{n,k}$ and then interference suppressing filter $\mathbf{z}_{n,k}$ (or $\mathbf{f}_k^o$) is applied. However, the coefficients $\mathbf{z}_{n,k}$ and $\mathbf{f}_k^o$ have different values. While $\mathbf{z}_{n,k}$ of the CE-based MMSE-TEQ depends on an instantaneous estimate of covariance matrix, $\mathbf{\Sigma}_{n,k}$, $\mathbf{f}_k^o$ of the LMS DA-TEQ depends on an (ensemble) covariance matrix of the signal $\bar{\mathbf{s}}_n$. The reason for this discrepancy is that two TEQ algorithms rely on different criteria: conditional versus unconditional MSE. As a result, the DA-TEQ algorithm does not fully exploit time-varying (second-order) statistics of the symbols $\mathbf{\Sigma}_{n,k}$ obtained from the channel decoder. Note that two filter coefficients $\mathbf{z}_{n,k}$ and $\mathbf{f}_k^o$ turn out to be equal only when $\sigma_g^2 = 0$ or $\sigma_g^2 \to \infty$. Now, we derive the MSE of the LMS DA-TEQ algorithm. In general, the steady-state MSE of an adaptive equalizer can be separated into a minimum MSE $\mathcal{M}_k^{\min}$ determined by the optimal Wiener solution and an excess MSE $\mathcal{M}_k^{\text{excess}}$ due to misadjustment of filter adaptation [23]. Accordingly, the MSE for the LMS DA-TEQ technique is given by

$$E[|s_{n,k} - \hat{s}_{n,k}^{\text{LMS-DA}}|^2] = \mathcal{M}_k^{\min} + \mathcal{M}_k^{\text{excess}} \tag{20}$$

where

$$\begin{aligned}\mathcal{M}_k^{\min} = 1 - &\mathbf{h}_{n,k}^H \\ &\times \left(\mathbf{h}_{n,k}\mathbf{h}_{n,k}^H + (1-\sigma_{\bar{s}}^2)\mathbf{H}_{n,1:k-1}\mathbf{H}_{n,1:k-1}^H\right. \\ &\left. + \left(1-\sigma_{\bar{s}}^2\right)\mathbf{H}_{n,k+1:K}\mathbf{H}_{n,k+1:K}^H + \mathbf{R}\right)^{-1}\mathbf{h}_{n,k}\end{aligned} \tag{21}$$

and

$$\mathcal{M}_k^{\text{excess}} \approx \frac{\xi\mathcal{M}_k^{\min}\left(\text{tr}\left(\mathbf{H}_n\mathbf{H}_n^H + \mathbf{R}\right) + \sigma_{\bar{s}}^2(K-1)\right)}{2} \tag{22}$$

where ξ is a step size of the LMS DA-TEQ technique. Derivation of (22) is presented in Appendix II. We can also compare the MSEs achieved by the DA-TEQ and MMSE-TEQ, that is, (16) versus (20). Even in the absence of channel estimation error and adaptation error, i.e., $E[\mathbf{E}_n\mathbf{E}_n^H] = 0$ and $\mathcal{M}_k^{\text{excess}} = 0$, the MSE expressions look different.

In Fig. 6, we investigate how the MSEs in (16) and (20) behave in terms of σ_g^2. We consider the single-input–single-output setup, i.e., $L = M = 1$ and QPSK modulation. We also consider a time-invariant channel response shown in Fig. 5. The signal-to-noise ratio (SNR) is set to 0 dB. We assume that the step sizes of the LMS channel estimator and the LMS DA-TEQ algorithm are set to $\xi = \xi_{\text{ch}}$ equally. In Fig. 6(a), the plots of MSE versus σ_g^2 are provided for the step size $\xi = \xi_{\text{ch}} = 0.0002$. Note that the MSE gap between two TEQ algorithms decreases when the *a priori* LLRs delivered from the channel decoder become stronger, i.e., $\sigma_g^2 \to \infty$. Hence, we expect that the performance gap between two TEQs would diminish after a sufficient number of iterations. Fig. 6(b) and (c) shows the plot of MSE for $\xi = \xi_{\text{ch}} = 0.0005$ and $\xi = \xi_{\text{ch}} = 0.001$, respectively. Due to larger step size, the channel estimation errors and excess MSE of the DA-TEQ algorithm increase. In this case, the performance gap between two TEQ algorithms increases. This implies that the DA-TEQ algorithm is more sensitive to the LMS adaptation errors than the CE-based MMSE-TEQ. Nevertheless, for the moderate range of step size 0.0002–0.001, the MSE gap between two equalizers decreases as σ_g^2 increases.

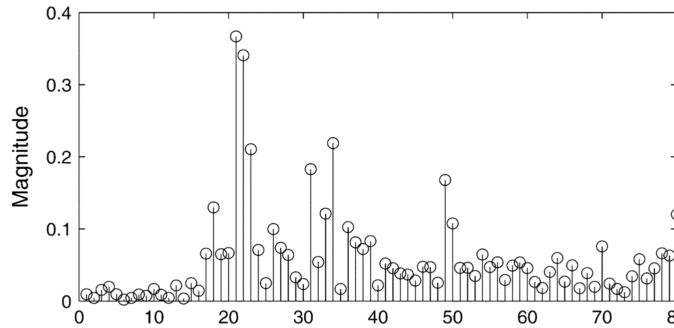

Fig. 5. Magnitude of the channel response obtained from a ten thousandth snapshot of underwater channels in Fig. 1.

B. EXIT Chart Analysis

The iterative behavior of TEQ algorithms can be well illustrated by an EXIT chart [7], [30]. In the EXIT chart, mutual information (MI) transfer curves of an equalizer and a channel decoder are drawn in the same axis to show the exchange of the MI between them. Note that the output MI ($I_{\text{Eq,output}}$) is drawn in terms of the input MI ($I_{\text{Eq,out}}$) for the equalizer while the output MI ($I_{\text{Dec,in}}$) is drawn in terms of the output MI ($I_{\text{Eec,out}}$) for the channel decoder.

In Fig. 7(a) and (b), the EXIT charts of two equalizers are provided along with that of the (133, 171) recursive systematic convolutional (RSC) code. We use the same setup as for the MSE analysis except that the step sizes of the LMS channel estimator and the LMS DA-TEQ are set to $\xi = \xi_{\text{ch}} = 0.001$. As for the DA-TEQ technique, the steady-state coefficients are expressed as $\mathbf{f}_{n,k} = \mathbf{f}_k^o + \Delta\mathbf{f}_{n,k}$ and $\mathbf{g}_{n,k} = \mathbf{g}_k^o + \Delta\mathbf{g}_{n,k}$, where $\mathbf{f}_k^o$ and $\mathbf{g}_k^o$ are Wiener solutions and $\Delta\mathbf{f}_{n,k}$ and $\Delta\mathbf{g}_{n,k}$ are the perturbation due to misadjustment errors. Assuming that the perturbation is jointly Gaussian, the coefficients of the LMS DA-TEQ are generated from the distribution

$$\begin{bmatrix}\mathbf{f}_{n,k}\\ \mathbf{g}_{n,k}\end{bmatrix} \sim \mathcal{CN}\left(\begin{bmatrix}\mathbf{f}_k^o\\ \mathbf{g}_k^o\end{bmatrix}, \frac{\mu}{2}\mathcal{M}_k^{\min}\mathbf{I}_{N+K-1}\right). \tag{23}$$

See Appendix I for the derivation of (23). For each value of input MI, the output MI for each equalizer is obtained via a histogram-based numerical method [7]. Comparing the trajectories between the equalizer curve and the decoder curve in Fig. 7, we observe that the MI transfer curves of both TEQ techniques approach similar output MI values as the input MI approaches one (see the points A and B in the charts). As long as SNR is high enough to create a tunnel between the equalizer curve and decoder curve, the actual performance achieved by both TEQs would not be much different after a sufficient number of iterations. On the other hand, the LMS DA-TEQ algorithm requires more iterations for convergence and a higher SNR to achieve convergence beyond the waterfall region, i.e., it has a higher SNR threshold.

V. Underwater Acoustic Communication Receiver Based on LMS DA-TEQ Technique

In this section, we introduce a receiver architecture built upon the LMS DA-TEQ technique. The block diagrams of

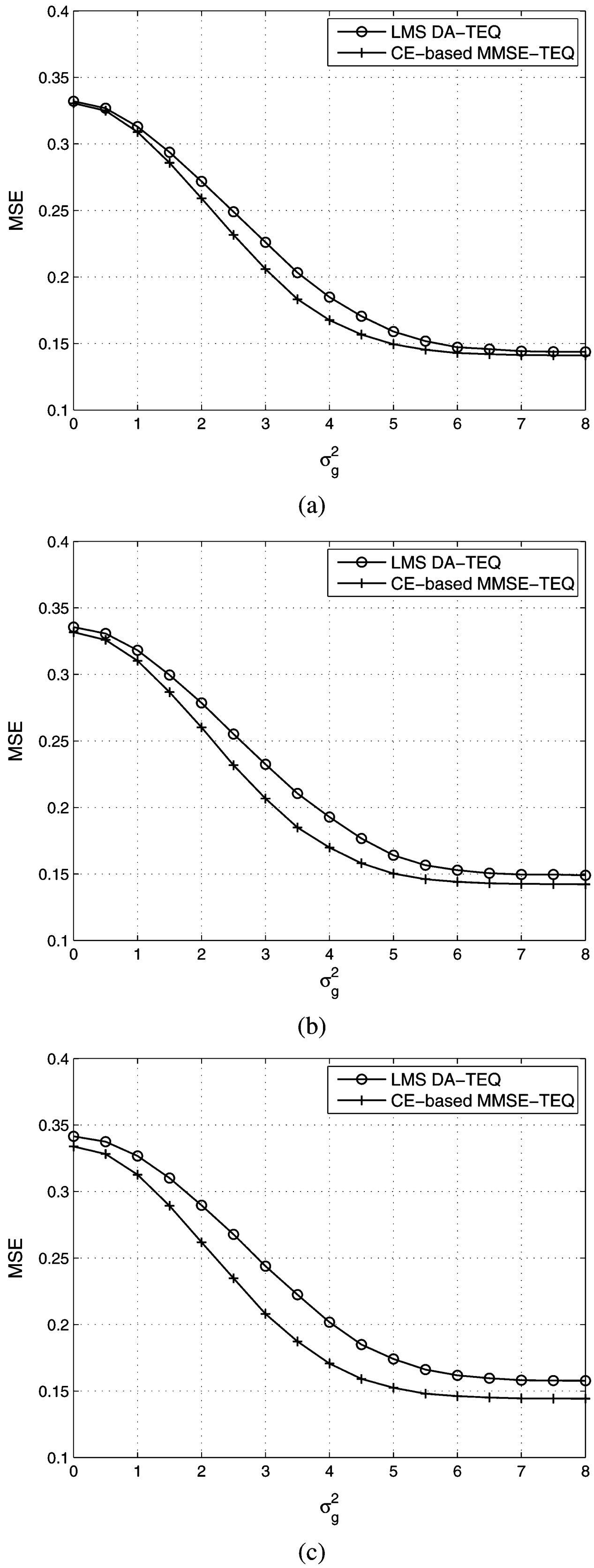

Fig. 6. Average MSEs of the MMSE-TEQ and the LMS DA-TEQ (a) for the step size $\xi = \xi_{\rm ch} = 0.0002$, (b) $\xi = \xi_{\rm ch} = 0.0005$, and (c) $\xi = \xi_{\rm ch} = 0.001$. The SNR is set to 0 dB.

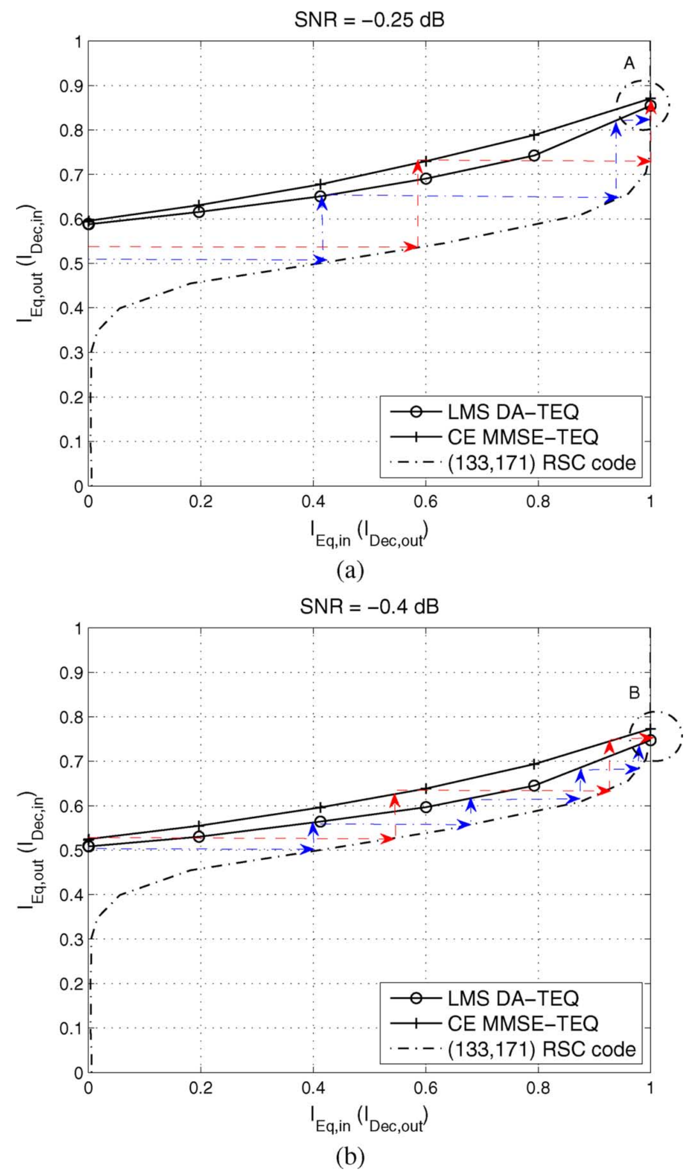

Fig. 7. Exit chart graphs of the MMSE-TEQ and the LMS DA-TEQ for (a) SNR $= -0.25$ dB and (b) SNR $= -0.4$ dB.

the underwater receiver for the $N_r \times 1$ single-input–multiple-output (SIMO) and the $N_r \times 2$ MIMO systems are depicted in Fig. 8(a) and (b), respectively. The received data at each hydrophone array element are processed by the synchronization block. The symbol timing, the start of the processing frame, and the channel length are estimated by thresholding the magnitude of correlation between the received samples and preamble data. The threshold is determined based on the relative magnitude of correlations measured in the silent period and preamble period. To align the data frame of all channels, we obtain a rough estimate of channel support by thresholding the magnitude of correlation. Once each data stream is aligned, phase distortion due to Doppler effect is compensated [27] and the LMS DA-TEQ algorithm is applied. Using the symbol estimates obtained by the LMS DA-TEQ, the extrinsic LLRs are obtained by the soft-input–soft-output demapper block. When there are multiple transmitter array elements, i.e., $N_t > 1$, the multiple streams of the extrinsic LLRs are multiplexed into a single stream via the parallel-to-serial converter. The remaining steps were explained in Section II-C.

A. Tracking Performance Enhancement

Generally, the LMS adaptive equalizer suffers from slow convergence. In shallow water, channel dynamics tend to change rapidly in local scale so that the statistic of channel gains is highly nonstationary [31]. Consequently, the LMS algorithm often fails to converge to steady state within the period over which the channel is stationary and hence the equalization performance is degraded. The slow convergence of the LMS algorithm is improved by employing the following methods.

First, we partition the whole frame into multiple sub-blocks over each of which the channel is assumed to be stationary. For each sub-block, we repeat the weight update of the (normalized) LMS algorithm until the filter weights converge to a steady state. At each repetition (called "pass"), the step size μ is decreased by the factor of $\rho(<1)$. For each pass, the equalizer coefficients are initialized by the last update in the previous pass. Denoting B as the size of the sub-block and J as a total number of repetitions per sub-block, the repeated weight update algorithm is summarized as follows.

for $t = 1 : D$,

  Set $\xi = \xi_{\text{init}}$.

  for $i = 1 : J$

    for $n = (t-1)B + 1 : tB$

      Let $e_{n,k} = s_{n,k} - \hat{s}_{n,k}^{\text{LMS}-\text{DA}}$.

      For all k, compute

$$\begin{bmatrix} \mathbf{f}_{n+1,k} \\ \mathbf{g}_{n+1,k} \end{bmatrix} = \begin{bmatrix} \mathbf{f}_{n,k} \\ \mathbf{g}_{n,k} \end{bmatrix} + \frac{\xi e_{n,k} \left[\mathbf{y}_n \quad \bar{\mathbf{s}}_{n,1:k-1} \quad \bar{\mathbf{s}}_{n,k+1:K} \right]^T}{\epsilon + \|\mathbf{y}_n\|^2 + \|\bar{\mathbf{s}}_{n,1:k-1}\|^2 + \|\bar{\mathbf{s}}_{n,k+1:K}\|^2}$$

    end

    Set $\xi \leftarrow \rho\xi$. For all k, set $\mathbf{f}_{(t-1)B+1,k} \leftarrow \mathbf{f}_{tB,k}$, and $\mathbf{g}_{(t-1)B+1,k} \leftarrow \mathbf{g}_{tB,k}$.

  end

end

DB becomes the length of the whole frame $(= T(M_t + M_d))$ and ξ_{init} is the initial step size. For better tracking performance, we employ an ϵ-normalized LMS algorithm [32]. A training symbol is used in place of $s_{n,k}$ in the training mode, and a tentative symbol estimate $Q(\hat{s}_{n,k}^{\text{LMS}-\text{DA}})$ in the detection mode. Note that the size of sub-block B should be chosen carefully such that the channel is stationary within the sub-block and sufficient data statistics are captured to find a useful solution via the adaptive algorithm.

Next, we exploit the sparse structure of the underwater channel to reduce the number of active equalizer coefficients. By reducing the number of unknown parameters that should be tracked by the equalizer, convergence speed of the equalizer can be enhanced. We extend the sparse equalization technique developed for the conventional DFE in [33] to the LMS DA-TEQ algorithm. Specifically, we first employ an LMS channel estimator to obtain a rough estimate of channels during the training period and order the channel taps in terms of the average power. We select the γ strongest taps, where γ is chosen such that the difference between the original MSE and the MSE obtained after active channel tap selection is less than P percent of the original MSE for some γ. After the sparse channel structure is identified, a portion of the support of the feedforward and feedback taps are switched off depending on the sparse structure found. The sparse structure directly indicates which elements of the feedback weight vector should be eliminated. More specifically, the feedback taps not contributing to the output due to zero channel gains are deactivated. On the contrary, the feedforward equalizer taps should be switched off at the cost of performance loss since all transmitted symbols contribute to each received sample through convolution. We preserve the matched filter property of the equalizer so that the feedforward coefficients corresponding to zero channel taps reflected on $\mathbf{r}_n$ are turned off.

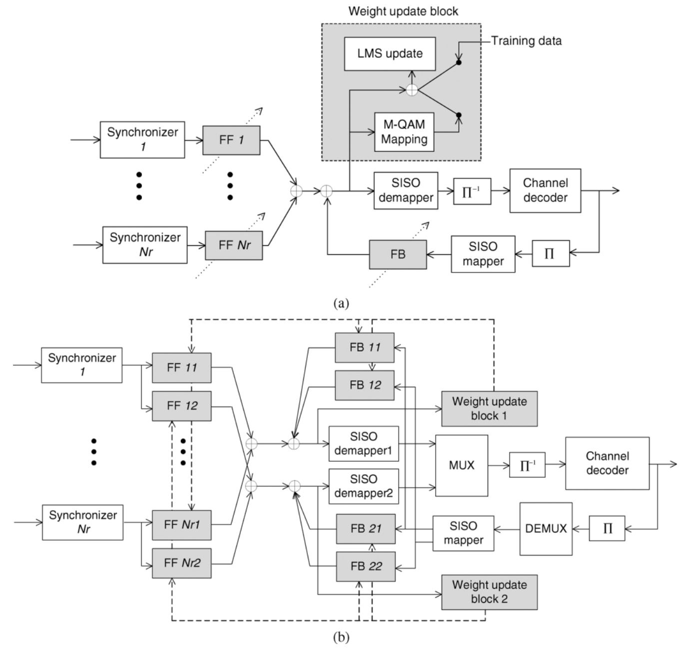

Fig. 8. Structure of underwater receiver based on the LMS DA-TEQ for (a) $N_r \times 1$ SIMO and (b) $N_r \times 2$ MIMO systems.

B. Soft-Input–Soft-Output Demapper

The LMS DA-TEQ technique cannot directly compute $\mu_{n,k}$ and $\sigma_{n,k}^2$ in (9) due to the absence of the channel estimate. The soft-input–soft-output demapper estimates $\mu_{n,k}$ and $\sigma_{n,k}^2$ and produces the extrinsic LLRs using them. From (2) and (13), the output of the LMS DA-TEQ algorithm is expressed as

$$\hat{s}_{n,k}^{\text{LMS}-\text{DA}} = \mathbf{f}_{n,k}^H(\mathbf{H}_n\mathbf{s}_n + \mathbf{n}_n) + \mathbf{g}_{n,k}^H \begin{bmatrix} \bar{\mathbf{s}}_{n,1:k-1} \\ \bar{\mathbf{s}}_{n,k+1:K} \end{bmatrix} \quad (24)$$

$$= \left(\mathbf{f}_{n,k}^H \mathbf{h}_{n,k}\right) s_{n,k} + \xi_{n,k} \quad (25)$$

where

$$\xi_{n,k} = \left(\mathbf{f}_{n,k}^H \mathbf{H}_n \begin{bmatrix} \mathbf{s}_{n,1:k-1} \\ 0 \\ \mathbf{s}_{n,k+1:K} \end{bmatrix} + \mathbf{f}_{n,k}^H \mathbf{n}_n + \mathbf{g}_{n,k}^H \begin{bmatrix} \bar{\mathbf{s}}_{n,1:k-1} \\ \bar{\mathbf{s}}_{n,k+1:K} \end{bmatrix}\right). \tag{26}$$

Note that the first and second terms in (25) are signal and residual noise components of the equalizer output, respectively. As long as the channel state remains constant and the coefficients $\mathbf{f}_{n,k}$ and $\mathbf{g}_{n,k}$ are in steady state, these terms are assumed to be stationary. If we view the expression (25) as $\mu_{t,k} s_n + \xi_{n,k}$ with $\mu_{n,k} = \mathbf{f}_{n,k}^H \mathbf{h}_{n,k}$ and $\sigma_{n,k}^2 = E[|\xi_{n,k}|^2]$, then we can estimate $\mu_{n,k}$ and $\sigma_{n,k}^2$ by time averaging

$$\hat{\mu}_{t,k}^{\text{LMS-DA}} = \frac{1}{B} \sum_{i=(t-1)B+1}^{tB} \frac{\hat{s}_{i,k}^{\text{LMS-DA}}}{Q\left(\hat{s}_{i,k}^{\text{LMS-DA}}\right)} \tag{27}$$

$$\left(\hat{\sigma}_{t,k}^{\text{LMS-DA}}\right)^2 = \frac{1}{B} \sum_{i=(t-1)B+1}^{tB} \left|\hat{s}_{i,k}^{\text{LMS-DA}} - \hat{\mu}_{k}^{\text{LMS-DA}} Q\left(\hat{s}_{i,k}^{\text{LMS-DA}}\right)\right|^2 \tag{28}$$

where $\hat{\mu}_{t,k}^{\text{LMS-DA}}$ and $(\hat{\sigma}_{t,k}^{\text{LMS-DA}})^2$ are the estimates of $\mu_{n,k}$ and $\sigma_{n,k}^2$ for the tth subblock and recall that $Q(\cdot)$ is the slicer operation. These estimates are derived from (25) assuming that $Q(\hat{s}_{i,k}^{\text{LMS-DA}}) \approx s_{n,k}$ for sufficiently high SNR. Note that these estimates are computed only for the coded symbols, not for the training symbols. Similar approach for estimating $\mu_{n,k}$ and $\sigma_{n,k}^2$ for feedforward TEQ was proposed in [21]. Since our LMS DA-TEQ exploits the soft feedback from the decoder, it uses only the coded symbols to obtain $\hat{\mu}_{t,k}^{\text{LMS-DA}}$ and $(\hat{\sigma}_{t,k}^{\text{LMS-DA}})^2$ while the approach in [21] can exploit the training data. Now we compute the extrinsic LLR for $\bar{c}_{n,k}^q$ as (29), shown at the bottom of the page.

VI. Experimental Results

In this section, we evaluate the performance of the LMS DA-TEQ-based receiver in real underwater environments. The SPACE 08 experiment was conducted off the coast of Martha's Vineyard, MA, during October 14–November 2, 2008. We compare the performance of the LMS DA-TEQ with that of the conventional LMS-DFE for a variety of configurations. In addition, the performance of the CE-based MMSE-TEQ is also included for several setups.[1]

A. Experiment Description

Over the whole experiment, we employ a $R_c = 1/2$ rate (131, 171) RSC code and a random interleaver of the size of 19 200–38 400 bits for data generation. Four transducers spaced by 50 cm are used for signal transmission and each of them has a frequency bandwidth of 9 kHz ($W = 4.5 \times 10^3$). The transducers and hydrophone array are all located on fixed tripods and hence there is little movement of the transmitter and the receiver. The carrier frequency is set to 13 kHz. The sampling rate of the transducer is 39.0625 ksamples/s and anti-aliasing filters with a cutoff frequency of about 18 kHz are used. Four 1-min data files are transmitted every 2 h and data transmissions are carried out 149 times during 14 days. For convenience, each transmission is indexed with "epoch 1–149."[2] Each of four data files contains six "chunks" wherein each chunk corresponds to 8-s samples of the received data (associated with each configuration). The transmitted data are received by several hydrophone arrays which are located at the range of 60, 200, and 1000 m. Once data transmission is finished every 2 h, ambient noise is recorded separately.

B. Parameter Setup

A square-root raised cosine filter with a rolloff factor $\beta = 0.2$ is used both in the transmitter and the receiver. A frame consists of six sets of training symbols and data symbols. Turbo iteration is carried out on a frame-by-frame basis. The length of training period is $M_t = 400$ and the length of data period is $M_d = 1600$. The length of preamble period is $M_p = 1000$. The preamble data are inserted at the start of each chunk. The data rate of the system can be obtained as

$$\frac{M_d}{M_t + M_d} \frac{39.06 \times 10^3}{\text{OVF}} N_t Q R_c \tag{30}$$

where OVF is the oversampling factor that represents the number of samples per symbol, i.e., sampling rate $=$ OVF $\times$ symbol rate.[3] The system bandwidth is given by

[1]We measured the performance of MMSE-TEQ only for the selected test cases since it took too long to process all data.

[2]In the SPACE 08 experiment, each epoch is distinguished by (Julian) date and time (in GMT) of the start of transmission. For example, the first epoch data corresponds to the data transmitted on the date 288 and the time 00:00. For the sake of brevity, we use the epoch index from 1 to 149 in the rest of the paper.

[3]For data transmission over a frequency band of $[-W, W]$ Hz, we define the bandwidth of the system as W Hz.

$$L_{\text{ext}}^{\text{LMS-DA}}\left(\bar{c}_{n,k}^q\right) = \ln \frac{\displaystyle\sum_{\theta \in \Theta_q^{+1}} \exp\left(-\frac{\left|\hat{s}_{n,k}^{\text{LMS-DA}} - \hat{\mu}_{t,k}^{\text{LMS-DA}}\theta\right|^2}{\left(\hat{\sigma}_{t,k}^{\text{LMS-DA}}\right)^2} + \frac{1}{2}\sum_{i=1, i\neq q}^{Q} \bar{c}_{n,k}^i L_{\text{pri}}(\bar{c}_{n,k}^i)\right)}{\displaystyle\sum_{\theta \in \Theta_q^{-1}} \exp\left(-\frac{\left|\hat{s}_{n,k}^{\text{LMS-DA}} - \hat{\mu}_{t,k}^{\text{LMS-DA}}\theta\right|^2}{\left(\hat{\sigma}_{t,k}^{\text{LMS-DA}}\right)^2} + \frac{1}{2}\sum_{i=1, i\neq q}^{Q} \bar{c}_{n,k}^i L_{\text{pri}}(\bar{c}_{n,k}^i)\right)}. \tag{29}$$

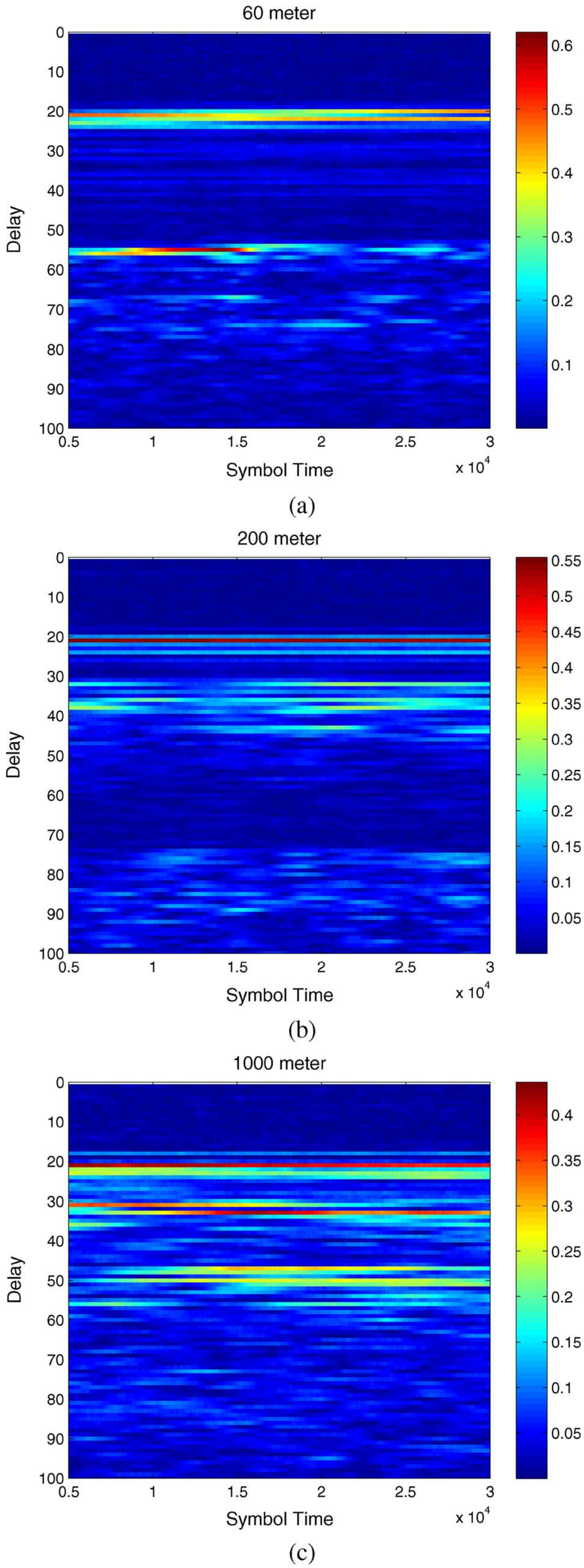

Fig. 9. Magnitude of channel impulse responses over time-delay domain for the distance of (a) 60 m, (b) 200 m, and (c) 1000 m.

$\min((1+\beta)39.06/2\ \mathrm{OVF}, 4.5)$ kHz. Hence, the over-Nyquist setup corresponds to the case where the symbol rate is larger than twice the positive bandwidth, i.e., $39.06/\mathrm{OVF} > 9$ Hz, equivalently for $\mathrm{OVF} = 2, 3$. The size of a sub-block is set to $B = 200$ (symbol periods) and a total number of repetitions for the weight update is set to $J = 5$. The initial step size is set to $\xi_{\mathrm{init}} = 0.01$ and it is decreased by $\rho = 0.8$ in every pass. The value of P for sparse equalization is set to 20%. We choose the equalizer length such that $L_p = K_f + 7$ and $L_f = K_p + 7$, where $K_f + K_p + 1$ are a maximum channel length. A noise power is estimated during the silent period. In SPACE 08, we observe that the phase compensation block does not help improving the performance of the equalizer. This would be why the receiver and the transmitter did not move so that gross Doppler effect did not exist. Hence, we turned off the phase compensation block while processing the field data obtained during SPACE 08.

C. *Experimental Results*

1) Underwater Channel Responses Versus Distance: In Fig. 9, underwater channel responses are shown for several distances. A recursive least square (RLS) channel estimator with a forgetting factor of 0.999 is employed. The symbol period is 102.4 μs. We observe that the main arrival paths appear at around 2-ms delay. The channel gains for the secondary arrivals fluctuate more rapidly. In addition, for longer distance, the time variation of the gains gets more significant. On the other hand, for the 60-m channel, the channel gains appear relatively calm and the response looks more sparse. For most cases, the actual channel span was around 6–7 ms corresponding to 60–70 channel taps for 9.77-ksymbols/s transmission.

2) Iterative Behavior of TEQ Receiver: First, we observe performance of the TEQ algorithms with iteration in real underwater channels. To evaluate the performance over different SNR levels, the separately recorded ambient noise was added to the received data. The symbol rate (=1/symbol period) is 9.77 ksymbols/s. Only 1000-m data for the epoch 24 are used for performance evaluation. Fig. 10(a)–(c) shows the plots of BER versus SNR for the 10×1 SIMO QPSK, the 10×1 SIMO 16-QAM, and the 10×2 MIMO QPSK transmissions, respectively. The data rates achieved by these systems are 3.66 kb/s for the 10×1 QPSK transmission and 7.32 kb/s for both 10×1 16-QAM and 10×2 QPSK transmissions. For comparison, the performance of the conventional LMS-DFE combined with Viterbi FEC decoder [33] is included.[4] The performance of the LMS DA-TEQ dramatically improves with iterations so that significant performance gain is achieved over the conventional LMS-DFE after the six iterations. The LMS DA-TEQ outperforms the LMS-DFE even before the first iteration due to the LMS-DFE suffering from severe error propagation in the decision-feedback process especially for long channel responses. Comparing the 10×1 16-QAM and 10×2 QPSK setups achieving the same data rate (= 7.32 kb/s), the performance of the LMS DA-TEQ algorithm is better for the 10×2 QPSK case. This suggests that increasing spatial dimension offers better error performance than increasing

[4]In this LMS-DFE algorithm, we did not limit the number of symbols that are fed back to the equalizer. Instead, the actual symbols to be fed back are chosen depending on a sparse structure of underwater channels. In fact, all postcursor symbols are considered as a candidate for feedback.

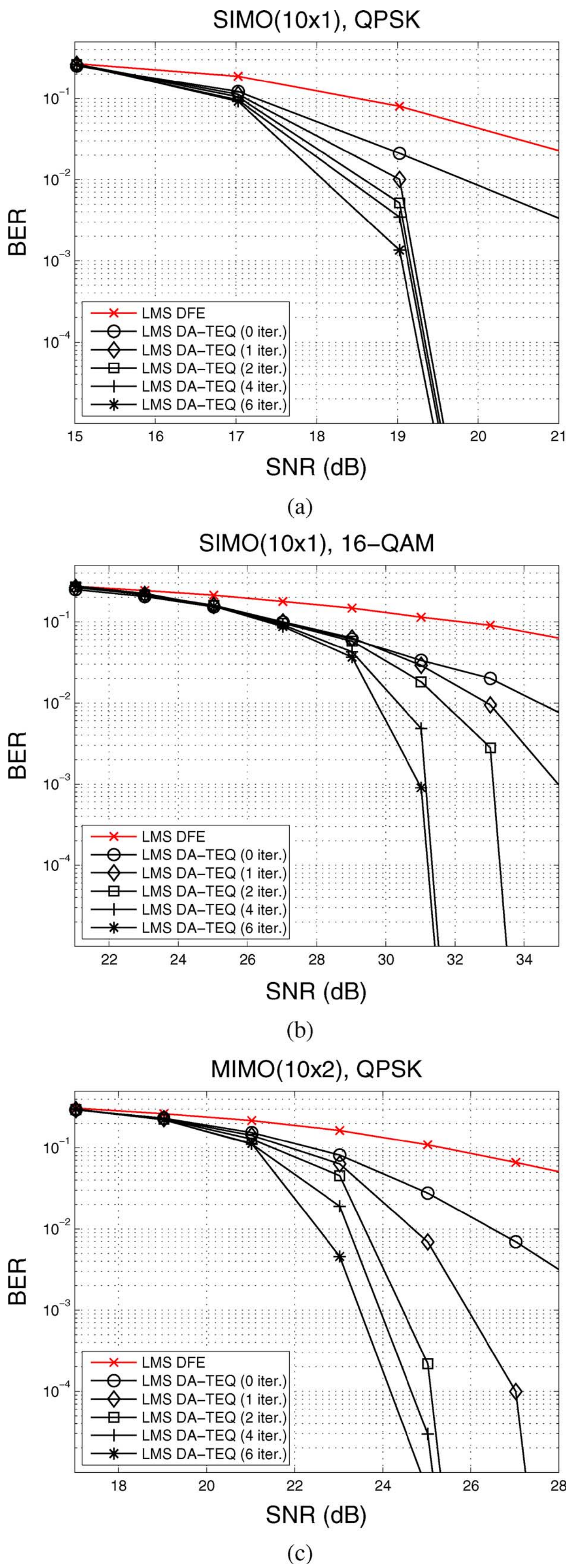

Fig. 10. Performance of LMS-DFE and LMS DA-TEQ for (a) 10×1 SIMO QPSK, (b) 10×1 SIMO 16-QAM, and (c) 10×2 MIMO QPSK transmissions.

modulation order. However, the performance for the 10×2 MIMO setup converges at the slowest speed among three cases.

3) Long-Term Experimental Results: Next, we present more extensive results measured for longer time durations (the epochs from 9 to 31). The symbol rate is fixed to 9.77 ksymbols/s, i.e., OVF $= 4$. Tables I–III present the BER performance for every four epochs of three equalizers: 1) LMS-DFE, 2) LMS DA-TEQ, and 3) CE-based MMSE-TEQ.[5] The environment logs including wave height and wind speed are also provided in Table IV. Different sizes of hydrophone arrays are used for each distance data, i.e., $N_r = 6, 8$, and 12 for 60, 200, and 1000 m, respectively. As for the LMS DA-TEQ and CE-based MMSE-TEQ, the performance is measured after the sixth iteration. Due to the tremendous amount of simulation time in the CE-based MMSE-TEQ algorithm, we could not provide the results for all setups. In all cases considered, the LMS DA-TEQ algorithm outperforms the conventional LMS-DFE by more than an order of magnitude. In many epochs, the LMS DA-TEQ could decode the data without errors while the LMS-DFE could not. In particular, the performance gain is remarkable for the $N_r \times 2$ MIMO setup where the problem size is twice that in the other SIMO setups. In most cases, the performance of the LMS DA-TEQ algorithm is comparable to that of the CE-based MMSE-TEQ algorithm. For some setups, the CE-based MMSE-TEQ algorithm is even worse than the LMS DA-TEQ, which is a counterintuitive from our analysis in Section IV. This appears to be due to inaccurate estimation of the covariance matrix of the noise plus residual signal in the CE-based MMSE-TEQ, which was not accounted for in the analysis. The CE-based MMSE-TEQ estimates $E[\mathbf{E}_n\mathbf{E}_n^H] + \mathbf{R}$ using (11) and this was performed only in the training period to keep the covariance matrix estimation errors and the data detection errors from causing error propagations. Due to the insufficient training symbols and inability to track the changes of the covariance matrix, accurate estimate of covariance matrix could not be obtained. We observed that the CE-based MMSE-TEQ is, in particular, sensitive to various mismatches in terms of channel length estimation, frame alignment, and covariance matrix estimation compared to the LMS DA-TEQ.

Another interesting point observed in these results is that the performance of the equalizers for the 200-m distance is often better than that for the 60-m distance. This observation can be explained by the shape of the channel responses shown in Fig. 9. Though the channel for the 60-m distance looks relatively calm, longer channel delay spread is generated and the magnitude of the secondary arrivals is larger. This makes the 60-m channel more challenging. For 1000-m distance, the LMS DA-TEQ performs well for most of cases. However, the performance is not good during epochs 17–20, where the wave height and wind speed are highest among all epochs (see Table IV). It is shown again that the performance of the LMS DA-TEQ for the $N_r \times 2$ QPSK case is better that for the $N_r \times 1$ 16-QAM case. (Both setups support the same data rate.) On the other hand, the performance of the conventional LMS-DFE is not satisfactory for either setup.

4) Performance Versus Symbol Rate: We look at how the throughput and performance of the LMS DA-TEQ vary in terms of different symbol rates and modulation orders. The BER av-

[5]The BER in the tables is averaged over set of four epochs.

TABLE I
EXPERIMENTAL RESULTS FOR 60-m DISTANCE ($N_r = 6$)

System	Setup	Data rate (kbit/s)	LMS-DFE	LMS DA-TEQ	CE MMSE-TEQ
Epoch 9 - 12	$N_r \times 1$ QPSK	3.66	0	0	0
	$N_r \times 1$ 16-QAM	7.32	4.21×10^{-2}	0	1.98×10^{-2}
	$N_r \times 2$ QPSK	7.32	8.24×10^{-3}	0	N/A
Epoch 13 - 16	$N_r \times 1$ QPSK	3.66	2.97×10^{-5}	0	0
	$N_r \times 1$ 16-QAM	7.32	1.56×10^{-1}	5.48×10^{-2}	6.25×10^{-2}
	$N_r \times 2$ QPSK	7.32	1.43×10^{-1}	9.82×10^{-3}	N/A
Epoch 17 - 20	$N_r \times 1$ QPSK	3.66	1.77×10^{-4}	0	1.12×10^{-4}
	$N_r \times 1$ 16-QAM	7.32	1.92×10^{-1}	1.67×10^{-1}	1.57×10^{-1}
	$N_r \times 2$ QPSK	7.32	1.59×10^{-1}	2.97×10^{-3}	N/A
Epoch 21 - 24	$N_r \times 1$ QPSK	3.66	9.48×10^{-6}	0	N/A
	$N_r \times 1$ 16-QAM	7.32	1.51×10^{-1}	4.67×10^{-2}	N/A
	$N_r \times 2$ QPSK	7.32	9.05×10^{-2}	0	N/A
Epoch 25 - 28	$N_r \times 1$ QPSK	3.66	1.71×10^{-4}	0	N/A
	$N_r \times 1$ 16-QAM	7.32	1.82×10^{-1}	2.31×10^{-2}	N/A
	$N_r \times 2$ QPSK	7.32	1.38×10^{-1}	2.67×10^{-2}	N/A
Epoch 29 - 31	$N_r \times 1$ QPSK	3.66	0	0	N/A
	$N_r \times 1$ 16-QAM	7.32	1.13×10^{-1}	4.73×10^{-2}	N/A
	$N_r \times 2$ QPSK	7.32	8.26×10^{-2}	9.92×10^{-6}	N/A

TABLE II
EXPERIMENTAL RESULTS FOR 200-m DISTANCE ($L = 8$)

System	Setup	Data rate (kbit/s)	LMS-DFE	LMS DA-TEQ	CE MMSE-TEQ
Epoch 9 - 12	$N_r \times 1$ QPSK	3.66	0	0	0
	$N_r \times 1$ 16-QAM	7.32	2.03×10^{-2}	0	0
	$N_r \times 2$ QPSK	7.32	1.66×10^{-3}	0	N/A
Epoch 13 - 16	$N_r \times 1$ QPSK	3.66	0	0	0
	$N_r \times 1$ 16-QAM	7.32	1.64×10^{-2}	0	8.93×10^{-5}
	$N_r \times 2$ QPSK	7.32	1.86×10^{-2}	0	N/A
Epoch 17 - 20	$N_r \times 1$ QPSK	3.66	0	0	0
	$N_r \times 1$ 16-QAM	7.32	1.96×10^{-2}	0	1.55×10^{-3}
	$N_r \times 2$ QPSK	7.32	5.17×10^{-2}	0	N/A
Epoch 21 - 24	$N_r \times 1$ QPSK	3.66	0	0	N/A
	$N_r \times 1$ 16-QAM	7.32	6.82×10^{-3}	0	N/A
	$N_r \times 2$ QPSK	7.32	1.32×10^{-2}	0	N/A
Epoch 25 - 28	$N_r \times 1$ QPSK	3.66	0	0	N/A
	$N_r \times 1$ 16-QAM	7.32	1.25×10^{-2}	0	N/A
	$N_r \times 2$ QPSK	7.32	1.35×10^{-2}	0	N/A
Epoch 29 - 31	$N_r \times 1$ QPSK	3.66	0	0	N/A
	$N_r \times 1$ 16-QAM	7.32	5.50×10^{-3}	0	N/A
	$N_r \times 2$ QPSK	7.32	5.70×10^{-3}	0	N/A

eraged over a long period (epochs 109–114) is provided exclusively for the LMS DA-TEQ in Table V. Only the 10×1 SIMO case and 1000-m distance are considered. As shown in the table, after five iterations, the LMS DA-TEQ can retrieve the data without errors for all BPSK and QPSK cases. This implies that our system can achieve 14.65 kb/s rate (corresponding to the case of QPSK, 19.53 ksymbols/s) with low error probability. On the other hand, for the 16-QAM case, we could achieve perfect data recovery for 6.51-ksymbols/s case and 0.01 BER for 9.77-ksymbols/s case. However, for higher symbol rate, the

TABLE III
EXPERIMENTAL RESULTS FOR 1000-m DISTANCE ($L = 10$)

System	Setup	Data rate (kbit/s)	LMS-DFE	LMS DA-TEQ	CE MMSE-TEQ
Epoch 9 - 12	$N_r \times 1$ QPSK	3.66	0	0	0
	$N_r \times 1$ 16-QAM	7.32	6.55×10^{-2}	0	0
	$N_r \times 2$ QPSK	7.32	3.70×10^{-3}	0	N/A
Epoch 13 - 16	$N_r \times 1$ QPSK	3.66	2.38×10^{-4}	0	0
	$N_r \times 1$ 16-QAM	7.32	1.75×10^{-1}	5.26×10^{-2}	1.30×10^{-2}
	$N_r \times 2$ QPSK	7.32	8.48×10^{-2}	0	N/A
Epoch 17 - 20	$N_r \times 1$ QPSK	3.66	7.66×10^{-3}	0	1.72×10^{-4}
	$N_r \times 1$ 16-QAM	7.32	2.33×10^{-1}	1.44×10^{-1}	7.08×10^{-2}
	$N_r \times 2$ QPSK	7.32	2.22×10^{-1}	1.77×10^{-1}	N/A
Epoch 21 - 24	$N_r \times 1$ QPSK	3.66	2.38×10^{-3}	3.79×10^{-5}	N/A
	$N_r \times 1$ 16-QAM	7.32	1.44×10^{-1}	2.44×10^{-2}	N/A
	$N_r \times 2$ QPSK	7.32	7.04×10^{-2}	4.96×10^{-5}	N/A
Epoch 25 - 28	$N_r \times 1$ QPSK	3.66	1.52×10^{-4}	0	N/A
	$N_r \times 1$ 16-QAM	7.32	1.53×10^{-1}	1.96×10^{-2}	N/A
	$N_r \times 2$ QPSK	7.32	6.26×10^{-2}	0	N/A
Epoch 29 - 31	$N_r \times 1$ QPSK	3.66	0	0	N/A
	$N_r \times 1$ 16-QAM	7.32	1.03×10^{-1}	2.79×10^{-2}	N/A
	$N_r \times 2$ QPSK	7.32	2.57×10^{-2}	0	N/A

TABLE IV
EXPERIMENT ENVIRONMENTS AND CONDITIONS

	Epoch 9-12	Epoch 13-16	Epoch 17-20	Epoch 21-24	Epoch 25-28	Epoch 29-31
Wave height (meter)	0.6083	0.6917	**0.9583**	0.6500	0.4417	0.4111
Wind speed (meter/s)	1.1917	5.9083	**6.6750**	5.4917	6.0333	4.7111

TABLE V
PERFORMANCE OF THE LMS DA-TEQ FOR DIFFERENT SYMBOL RATES AND MODULATIONS (1000 m)

Modulation	Symbol rate (ksym/s)	Data rate (kbit/s)	No Iteration	Iteration 1	Iteration 2	Iteration 5
BPSK	6.51 (OVF=6)	2.44	0.0	0.0	0.0	0.0
	9.77 (OVF=4)	3.66	0.0	0.0	0.0	0.0
	19.53* (OVF=2)	7.32	0.0002	0.0	0.0	0.0
QPSK	6.51 (OVF=6)	4.88	0.0	0.0	0.0	0.0
	9.77 (OVF=4)	7.32	0.0	0.0	0.0	0.0
	19.53* (OVF=2)	**14.65**	0.310	0.004	0.002	0.0
16-QAM	6.51 (OVF=6)	9.77	0.01	0.0	0.0	0.0
	9.77 (OVF=4)	**14.65**	0.0211	0.0138	0.0108	0.0098
	19.53* (OVF=2)	29.27	0.48	0.49	0.51	0.55

data decoding was not successful. It is of particular interest to compare two cases: the QPSK, 19.53-ksymbols/s case and the 16-QAM, 9.77 ksymbols/s, where the highest data throughput (14.65 kb/s) is achieved among all setups. Note that the QPSK, 19.53-ksymbols/s case corresponds to the over-Nyquist setup, where the symbol rate is larger than the system bandwidth 9 kHz (we mark these setups using "*" in the table). We observe that the over-Nyquist transmission yielded better decoding performance than that with the increased modulation order and the LMS DA-TEQ could maintain good decoding performance even for over-Nyquist setups.

VII. CONCLUSION

In this paper, we have investigated linear turbo equalizers for underwater acoustic communications. Specifically, we studied a low-complexity TEQ technique to the single-carrier equalization of underwater channels. The two linear TEQ techniques, CE-based MMSE-TEQ and LMS DA-TEQ, were considered. Clearly, the complexity of the LMS DA-TEQ is much lower than the CE-based MMSE-TEQ. We showed that both TEQ techniques would show comparable performance as the number of iterations increases. Inspired by the small performance gap of both TEQs after a sufficient number of iterations, we built an underwater receiver architecture based on the LMS DA-TEQ technique. According to the actual in-water experiments conducted off the coast of Massachusetts, the LMS DA-TEQ technique could achieve the data throughput of 15 kb/s with low probability of error. In addition, the performance of the LMS DA-TEQ is an order of magnitude better than that of the conventional LMS decision feedback equalizer [27] for a variety of configurations such as different times, distances, and symbol rates.

APPENDIX I
DERIVATION OF (23)

We derive a covariance matrix of the perturbation noise in LMS filter coefficients following the convergence analysis in [23]. Let filter coefficients, input signal, and desired signal of an LMS adaptive filter be $\mathbf{w}_n$, $\mathbf{u}_n$, and d_n, respectively. The LMS update rule is given by

$$\mathbf{w}_{n+1} = \mathbf{w}_n + \xi \mathbf{u}_n (d_n - \mathbf{w}_n^H \mathbf{u}_n)^*. \tag{31}$$

A Wiener solution of this adaptive filter is given by $\mathbf{w}_o = \mathrm{Cov}(\mathbf{u}_n)^{-1}\mathrm{Cov}(\mathbf{u}_n, d_n)$. Denoting an error signal as $\epsilon_n = d_n - \mathbf{w}_o^H \mathbf{u}_n$, we can show that

$$E[|\epsilon_n|^2] = \sigma_d^2 - \mathrm{Cov}(\mathbf{u}_n, d_n)^H \mathrm{Cov}(\mathbf{u}_n)^{-1}\mathrm{Cov}(\mathbf{u}_n, d_n)$$

[23]. Hence, $\mathbf{w}_n - \mathbf{w}_o$ becomes a perturbation vector due to misadjustment errors of the adaptive filter. If we subtract $\mathbf{w}_o$ from both sides of (31), then the LMS weight update rule is written

$$\begin{aligned}
\mathbf{w}_{n+1} - \mathbf{w}_o &= \mathbf{w}_n - \mathbf{w}_o + \xi \mathbf{u}_n (d_n - \mathbf{w}_n^H \mathbf{u}_n)^* && (32)\\
&= \mathbf{w}_n - \mathbf{w}_o + \xi \mathbf{u}_n (\epsilon_n - (\mathbf{w}_n - \mathbf{w}_o)^H \mathbf{u}_n)^* && (33)\\
&= \left(\mathbf{I} - \xi \mathbf{u}_n \mathbf{u}_n^H\right)(\mathbf{w}_n - \mathbf{w}_o) + \xi \mathbf{u}_n \epsilon_n^*. && (34)
\end{aligned}$$

Using the direct-averaging method [23], we can approximate the solution of the difference equation in (34) as that of the equation

$$\mathbf{w}_{n+1} - \mathbf{w}_o = (\mathbf{I} - \xi \mathrm{Cov}(\mathbf{u}_n))(\mathbf{w}_n - \mathbf{w}_o) + \xi \mathbf{u}_n \epsilon_n^*. \tag{35}$$

Denoting $\mathbf{K}_n = \mathrm{Cov}(\mathbf{w}_n - \mathbf{w}_o)$ and from (35), we have

$$\begin{aligned}
\mathbf{K}_{n+1} = (\mathbf{I} - \xi \mathrm{Cov}(\mathbf{u}_n))&\mathbf{K}_n(\mathbf{I} - \xi \mathrm{Cov}(\mathbf{u}_n)) \\
&+ \xi^2 \mathrm{Cov}(\mathbf{u}_n) E[|\epsilon_n|^2]. \quad (36)
\end{aligned}$$

Since $\mathbf{K}_{n+1} = \mathbf{K}_n$ in steady state, (36) becomes

$$\begin{aligned}
\xi \mathrm{Cov}(\mathbf{u}_n)\mathbf{K}_n \mathrm{Cov}(\mathbf{u}_n) - \mathrm{Cov}(\mathbf{u}_n)\mathbf{K}_n &- \mathbf{K}_n \mathrm{Cov}(\mathbf{u}_n) \\
&= -\xi \mathrm{Cov}(\mathbf{u}_n) E[|\epsilon_n|^2]. \quad (37)
\end{aligned}$$

When the input signal $\mathbf{u}_n$ is white, i.e., $\mathrm{Cov}(\mathbf{u}_n) = \alpha \mathbf{I}$, $\mathbf{K}_n$ is obtained as

$$\begin{aligned}
\mathbf{K}_n &= \frac{\xi}{2 - \alpha\xi} E[|\epsilon_n|^2]\mathbf{I} && (38)\\
&\approx \frac{\xi}{2} E[|\epsilon_n|^2]\mathbf{I} && (39)
\end{aligned}$$

where (39) follows from the assumption that the step size ξ is small. Due to the assumption on the white input, this result can be used for the analysis of the adaptive channel estimator in Section IV-A.

On the other hand, for a correlated input, if we plug $\mathbf{K}_n = (\xi)/(2)E[|\epsilon_n|^2]\mathbf{I}$ into the left-hand side of (37), then it becomes $(1 - \xi/2)(-\xi \mathrm{Cov}(\mathbf{u}_n)E[|\epsilon_n|^2]) \approx -\xi \mathrm{Cov}(\mathbf{u}_n)E[|\epsilon_n|^2]$ for small ξ, which equals to the right-hand side. Hence, the solution (39) approximately holds for the correlated input as well. Hence, we can also use this result for the analysis of the LMS DA-TEQ in Section IV-B.

APPENDIX II
DERIVATION OF (22)

We derive the excess MSE of the LMS DA-TEQ using the results in [32, Sec. 6.5.6]. For sufficiently small ξ

$$\mathcal{M}_k^{\mathrm{excess}} \approx \frac{\xi \mathcal{M}_k^{\min} \mathrm{tr}\left(\mathrm{Cov}\left(\begin{bmatrix} \mathbf{y}_n \\ \bar{\mathbf{s}}_{n,k} \end{bmatrix}\right)\right)}{2}. \tag{40}$$

Since we have (41), shown at the bottom of the page, we have

$$\mathcal{M}_k^{\mathrm{excess}} \approx \frac{\xi \mathcal{M}_k^{\min} \left(\mathrm{tr}\left(\mathbf{H}_n \mathbf{H}_n^H + \mathbf{R}\right) + \sigma_{\bar{s}}^2 (K-1)\right)}{2}. \tag{42}$$

$$\mathrm{Cov}\left(\begin{bmatrix} \mathbf{y}_n \\ \bar{\mathbf{s}}_{n,k} \end{bmatrix}\right) = \begin{bmatrix} \mathbf{H}_n \mathbf{H}_n^H + \mathbf{R} & \sigma_{\bar{s}}^2 \left[\mathbf{H}_{n,1:k-1} \quad \mathbf{H}_{n,k+1:K}\right] \\ \sigma_{\bar{s}}^2 \left[\mathbf{H}_{n,1:k-1} \quad \mathbf{H}_{n,k+1:K}\right]^H & \sigma_{\bar{s}}^2 \mathbf{I}_{K-1} \end{bmatrix} \tag{41}$$

REFERENCES

[1] S. U. H. Qureshi, “Adaptive equalization,” *Proc. IEEE*, vol. 73, pp. 1349–1387, Sep. 1985.

[2] B. Li, S. Zhou, M. Stojanovic, L. Freitag, and P. Willett, “Multicarrier communication over underwater acoustic channels with nonuniform Doppler shifts,” *IEEE J. Ocean. Eng.*, vol. 33, no. 2, pp. 198–208, Apr. 2008.

[3] K. Fang, L. Rugini, and G. Leus, “Low-complexity block turbo equalization for OFDM systems in time-varying channels,” *IEEE Trans. Signal Process.*, vol. 56, no. 11, pp. 5555–5566, Nov. 2008.

[4] C. Berrou and A. Glavieux, “Near optimum error-correcting coding and decoding: Turbo-codes,” *IEEE Trans. Commun.*, vol. 44, no. 10, pp. 1261–1271, Oct. 1996.

[5] C. Douillard, M. Jezequel, C. Berrou, A. Picard, P. Didier, and A. Glavieux, “Iterative correction of intersymbol interference: Turbo-equalization,” *Eur. Trans. Telecommun.*, vol. 6, pp. 507–511, Sep./Oct. 1995.

[6] C. Laot, A. Glavieux, and J. Labat, “Turbo equalization: Adaptive equalization and channel decoding jointly optimized,” *IEEE J. Sel. Areas Commun.*, vol. 19, no. 9, pp. 1744–1751, Sep. 2001.

[7] M. T. Tuchler, R. Koetter, and A. C. Singer, “Turbo equalization: Principles and new results,” *IEEE Trans. Commun.*, vol. 50, no. 5, pp. 754–767, May 2002.

[8] M. T. Tuchler, A. C. Singer, and R. Koetter, “Minimum mean square error equalization using *a priori* information,” *IEEE Trans. Signal Process.*, vol. 50, no. 3, pp. 673–683, Mar. 2002.

[9] R. Otnes and M. Tuchler, “Iterative channel estimation for turbo equalization of time-varying frequency-selective channels,” *IEEE Trans. Wireless Commun.*, vol. 3, no. 6, pp. 1918–1923, Nov. 2004.

[10] A. Anastasopoulos and K. M. Chugg, “Adaptive soft-input soft-output algorithms for iterative detection with parametric uncertainty,” *IEEE Trans. Commun.*, vol. 48, no. 10, pp. 1638–1649, Oct. 2000.

[11] M. Nissila and S. Pasupathy, “Soft-input soft-output equalizers for turbo receivers: A statistical physics perspective,” *IEEE Trans. Commun.*, vol. 55, no. 7, pp. 1300–1307, Jul. 2007.

[12] X. Wang and H. V. Poor, “Iterative (turbo) soft interference cancellation and decoding for coded CDMA,” *IEEE Trans. Commun.*, vol. 47, no. 7, pp. 1046–1061, Jul. 1999.

[13] M. Sellathurai and S. Haykin, “Turbo-BLAST for wireless communications: Theory and experiments,” *IEEE Trans. Signal Process.*, vol. 50, no. 10, pp. 2538–2546, Oct. 2002.

[14] S. L. Ariyavisitakul, “Turbo space-time processing to improve wireless channel capacity,” *IEEE Trans. Commun.*, vol. 48, no. 8, pp. 1347–1359, Aug. 2000.

[15] B. Hochwald and S. T. Brink, “Achieving near-capacity on a multiple-antenna channel,” *IEEE Trans. Commun.*, vol. 51, no. 3, pp. 389–399, Mar. 2003.

[16] T. Oberg, B. Nilsson, N. Olofsoon, M. L. Nordenvaad, and E. Sangfelt, “Underwater communication link with iterative equalization,” in *Proc. IEEE OCEANS Conf.*, Sep. 2006, DOI: 10.1109/OCEANS.2006.307059.

[17] J. W. Choi, D. Drost, A. C. Singer, and J. Preisig, “Iterative multi-channel equalization and decoding for high frequency underwater acoustic communications,” in *Proc. 5th IEEE Sensor Array Multichannel Signal Process. Workshop*, Jul. 2008, pp. 127–130.

[18] R. Otnes and T. H. Eggen, “Underwater acoustic communications: Long-term test of turbo equalization in shallow water,” *IEEE J. Ocean. Eng.*, vol. 33, no. 3, pp. 321–334, Jul. 2008.

[19] S. Roy, T. M. Duman, V. McDounald, and J. G. Proakis, “High-rate communication for underwater acoustic channels using multiple transmitters and space-time coding: Receiver structures and experimental results,” *IEEE J. Ocean. Eng.*, vol. 32, no. 3, pp. 663–688, Jul. 2007.

[20] S. Roy, T. M. Duman, and V. K. McDonald, “Error rate improvement in underwater MIMO communications using sparse partial response equalization,” *IEEE J. Ocean. Eng.*, vol. 34, no. 2, pp. 181–201, Apr. 2009.

[21] P. van Walree and G. Leus, “Robust underwater telemetry with adaptive turbo multiband equalization,” *IEEE J. Ocean. Eng.*, vol. 34, no. 4, pp. 645–655, Oct. 2009.

[22] H. Wan, R.-R. Chen, J. W. Choi, A. Singer, J. Preisig, and B. Farhang-Boroujeny, “Markov chain Monte Carlo detection for underwater acoustic channels,” in *Proc. Inf. Theory Appl. Workshop*, Jan. 2010, DOI: 10.1109/ITA.2010.5454145.

[23] S. Haykin, *Adaptive Filter Theory*, 4th ed. Englewood Cliffs, NJ: Prentice-Hall, 2001.

[24] S. Roy and J. J. Shynk, “Analysis of the data-reusing LMS algorithm,” in *Proc. 32nd Midwest Symp. Circuits Syst.*, Aug. 1989, vol. 2, pp. 1127–1130.

[25] B. Widrow and S. D. Stearns, *Adaptive Signal Processing*. Englewood Cliffs, NJ: Prentice-Hall, 1985.

[26] R. H. Kwong and E. W. Johnston, “A variable step size LMS algorithm,” *IEEE Trans. Signal Process.*, vol. 40, no. 7, pp. 1633–1642, Jul. 1992.

[27] M. Stojanovic, J. Catipovic, and J. G. Proakis, “Phase-coherent digital communications for underwater acoustic channels,” *IEEE J. Ocean. Eng.*, vol. 19, no. 1, pp. 100–111, Jan. 1994.

[28] J. G. Proakis, *Digital Communication*, 4th ed. New York: McGraw-Hill, 2001.

[29] A. M. Tonello, “Space-time bit-interleaved coded modulation with an iterative decoding strategy,” in *Proc. IEEE Veh. Technol. Conf.*, Sep. 2000, pp. 473–478.

[30] S. ten Brink, “Convergence of iterative decoding,” *Electron. Lett.*, vol. 35, pp. 806–808, May 1999.

[31] W. Li and J. C. Preisig, “Estimation of rapidly time-varying sparse channels,” *IEEE J. Ocean. Eng.*, vol. 32, no. 4, pp. 927–939, Oct. 2007.

[32] A. H. Sayed, *Fundamentals of Adaptive Filtering*. New York: Wiley-Interscience, 2003.

[33] M. Kocic, D. Brady, and M. Stojanovic, “Sparse equalization for real-time underwater acoustic communications,” in *Proc. OCEANS Conf.*, Oct. 1995, pp. 1417–1422.

Jun Won Choi received the B.S. and M.S. degrees in electrical and computer engineering from Seoul National University, Seoul, Korea, in 2000 and 2002, respectively, and the Ph.D. degree in electrical and computer engineering from the University of Illinois at Urbana-Champaign (UIUC), Urbana, in 2010.

He was a summer intern at Intersymbol and Qualcomm Corp. R&D in 2005 and 2008, respectively. Currently, he is with Qualcomm QCT, San Diego, CA. His research area includes wireless/underwater communications, signal processing, graphical-model-based statistical inference, and low-power digital system design. Recently, he has been focusing on efficient design of iterative detection and decoding (IDD) algorithm for large size systems.

Thomas J. Riedl received the B.Sc. degree in electrical and computer engineering from the Technische Universität München, Munich, Germany, in 2008 and the M.Sc. degree in electrical and computer engineering from the University of Illinois at Urbana-Champaign (UIUC), Urbana, in 2009, where he is currently working towards the Ph.D. degree in the Department of Electrical and Computer Engineering. He is also a guest Ph.D. student in the School of Communication and Computer Sciences, Swiss Federal Institute of Technology (EPFL), Lausanne, Switzerland. His advisors are Prof. A. Singer and Prof. R. Urbanke.

His research interests are in signal detection and estimation and information theory.

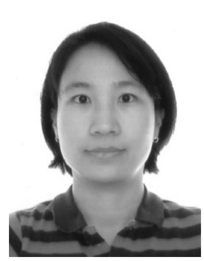

Kyeongyeon Kim (S’04–M’10) received the B.Sc., M.Sc., and Ph.D. degrees in electrical engineering from Yonsei University, Seoul, Korea, in 2001, 2003, and 2007, respectively.

As a Postdoctoral Researcher, she worked at Purdue University and University of Illinois at Urbana-Champaign. She is currently an R&D staff member with Samsung Advanced Institute of Technology (SAIT). Her research interests are in the fields of communication and signal processing, with particular emphasis on array signal processing, multiple-input–multiple-output (MIMO) transceiver design, turbo equalization, and soft-defined radio (SDR).

Andrew C. Singer (S'92–M'96–SM'05–F'10) received the S.B., S.M., and Ph.D. degrees in electrical engineering and computer science from the Massachusetts Institute of Technology (MIT), Cambridge.

After MIT, he was a Research Scientist at Sanders, A Lockheed Martin Company, Manchester, NH. Since 1998, he has been on the faculty at the University of Illinois at Urbana-Champaign, Urbana, where he is currently a Willet Faculty Scholar and Professor in the Department of Electrical and Computer Engineering. He is also a Research Professor, affiliated with the Signal Processing and Communications Groups in the Coordinated Science Laboratory. He is also the Director of the Technology Entrepreneur Center in the College of Engineering. In 2000, he cofounded Intersymbol Communications, Inc. [acquired by Finisar (FNSR) in 2007], a communications IC company specializing in integrated circuits for the optical communications industry. He serves on the board of directors of a number of technology companies and as an expert witness for electronics, communications, and circuit related technologies. His current research interests include statistical signal processing; wireless and underwater acoustic communications; LIDAR signal processing; adaptive filtering and machine learning; universal prediction, data compression, and universal methods; nonlinear dynamics and solitons; and financial modeling.

James C. Preisig (S'79–M'80) received the B.S. degree in electrical engineering from the United States Coast Guard Academy, New London, CT, in 1980, the S.M. and E.E. degrees in electrical engineering from the Massachusetts Institute of Technology (MIT), Cambridge, in 1988, and the Ph.D. degree in electrical and ocean engineering from the Massachusetts Institute of Technology/Woods Hole Oceanographic Institution (WHOI) Joint Program in Oceanography and Oceanographic Engineering, Cambridge, MA, in 1992.

He was a Postdoctoral Investigator at WHOI from 1992 to 1994 and a Visiting Assistant Professor at Northeastern University, Boston, MA, from 1994 to 1997. Since July 1997, he has been on the scientific staff of the Department of Applied Ocean Physics and Engineering, WHOI, and is currently an Associate Scientist with tenure. His research interests are in the areas of adaptive signal processing, system identification, underwater acoustic propagation modeling, underwater acoustic communications, and numerical optimization.

Dr. Preisig is the recipient of the 1999 U.S. Office of Naval Research Ocean Acoustics Young Faculty Award and is a member of the Acoustical Society of America's Underwater Acoustics and Signal Processing Technical Committees. He is also an Associate Editor of the IEEE JOURNAL OF OCEANIC ENGINEERING and served as a member of the IEEE Sensor Array and Multichannel Signal Processing Technical Committee from 1998 to 2004.